Eur. Phys. J. D **45**, 369–389 (2007)
DOI: 10.1140/epjd/e2007-00251-1

THE EUROPEAN PHYSICAL JOURNAL D

Non-equilibrium electron and phonon dynamics in metals under femtosecond laser pulses

L.D. Pietanza[1,a], G. Colonna[1], S. Longo[1,2], and M. Capitelli[1,2]

[1] Istituto di Metodologie Inorganiche e dei Plasmi (IMIP), CNR, sez. Bari, via Amendola 122/D, 70126 Bari, Italy
[2] Dipartimento di Chimica, Università degli Studi di Bari, via Orabona 4, 70126 Bari, Italy

Received 22 March 2007
Published online 10 August 2007 –

Abstract. Different models for relaxation dynamics of electrons and phonons in a thin metal film heated by femto-pico second laser pulses have been discussed. The traditional two-temperature approach reveals to be inaccurate due to deviations of electrons and phonons from Fermi-Dirac and Bose-Einstein distributions, respectively. Coupled Boltzmann kinetic equations have been adapted for the quantum statistics to study the energy distribution of electrons and phonons in metals. Theoretical details have been discussed and a new solution method has been proposed overcoming numerical problems and improving stability, allowing the study of the dynamics until the complete relaxation. Numerical results have been compared with photoemission spectroscopy experimental data.

PACS. 47.70.Nd Nonequilibrium gas dynamics – 52.38.Mf Laser ablation – 07.05.Tp Computer modeling and simulation

1 Introduction

Laser interaction with metallic surfaces is a topic of large interest for basic and applied research. A laser pulse of moderate fluence focused on the surface of a metallic target is absorbed by the electrons in the conduction band, leaving the lattice unperturbed due to its heat capacity, generating a non equilibrium condition in the solid. Transition to equilibrium is governed essentially by two processes: electron-electron ($e-e$) and electron-phonon ($e-p$) collisions. The first process forces the electron distribution towards the Fermi-Dirac distribution, without changing the overall amount of electron energy. This process, known as "internal thermalization", occurs on a time scale of hundreds of femtoseconds. On the other hand, $e-p$ collisions exchange energy between the perturbed electrons and the lattice. The excess of electron energy due to the laser absorption is thus transferred to the lattice, ending in local equilibrium in the metal. This process, called "external thermalization", has characteristic times that range from hundreds of femtoseconds to picoseconds.

The laser-induced perturbation and the material response strongly depend on the laser pulse duration in comparison with the characteristic collisional time scales. For a nanosecond laser pulse, local equilibrium is achieved during the laser pulse and the metal thermodynamic state is described by one temperature [1]. With a picosecond laser, before the pulse end, the electron gas achieves internal thermalization while the electron-lattice system is still far from equilibrium. In these conditions the classical two-temperature model (TTM) [2,3] is used, which assigns a different temperature to electrons (T_e) and phonons (T_L), whose time evolution is governed by the $e-p$ energy exchange. The energy exchange rate is assumed proportional to the temperature difference and to a coupling constant [2,3].

When a femtosecond laser pulse is used, $e-e$ collisions are not fast enough to thermalize the electron gas during the laser pulse, and electron distribution departures from non-equilibrium conditions are maintained up to some hundreds of femtoseconds. In this condition, the TTM approach is inadequate and microscopic kinetic approach should be used. The Boltzmann equation should be solved for the electron and phonon gas, calculating the energy distribution for the two systems.

In this work, electron and phonon relaxation dynamics, after femtosecond laser perturbation, has been investigated through the numerical solution of the system of electron and phonon Boltzmann equations. In this way, the simultaneous time evolution of electron and phonon distributions, during and after the laser perturbation, can be calculated, emphasising non-equilibrium effects.

Several theoretical works have been devoted to this problem [4–11], using different approaches in considering laser absorption and in calculating collisional contributions. While all the authors describe the $e-e$ collisions in the same way through detailed collision integrals, $e-p$

[a] e-mail: daniela.pietanza@ba.imip.cnr.it

interactions have been described differently. Sun et al. [4] take into account $e-p$ collisions in the relaxation time approximation approach, in which a macroscopic relaxation time of $\tau_p = 1$ ps is imposed. Del Fatti [5], instead, calculates $e-p$ interaction through a detailed collision integral, but using the acoustic deformation potential approach for the $e-p$ matrix. Rethfeld et al. [10], instead, calculate the $e-p$ matrix including the electron gas screening effect, while Groenveld et al. [6] take into account the electron gas screening in the limit of small-wave-number.

The laser perturbation is considered as a single photon absorption that induces a transition in the electron energy space from E_i to $E_i + h\nu_{las}$. Some authors [4,5] consider all the radiation absorbed by the metal, while, more accurate models calculate an absorption coefficient obtained by using a resonant dipole transition [7] as well as a dipole transition mediated by phonon collisions [9,10]. With the only exception of Rethfeld's model [10], phonon distribution is considered a constant Bose-Einstein at the initial metal temperature.

In the present work, both $e-e$ and $e-p$ collision processes have been described by detailed collision integrals [11–14]. $e-p$ collision integrals have been calculated considering the screening of the electron gas and the laser absorption as been included as in references [4,5].

Theoretical works can be validated by experimental investigations, such as photoemission spectroscopy (time-resolved two-photon photoemission experiments, 2PPE) [15–26] and pump-and-probe reflectivity and transmissivity measurements [4–6,27–40] performed using femtosecond lasers. This last technique gives hints on nonequilibrium conditions, but the sensitivity to electron and phonon distribution details is poor. These experiments have verified the electron gas non-equilibrium, providing the $e-p$ coupling constant "g", used in the TTM approach, for different materials [27,29].

On the other hand, 2PPE [15–26] directly measure the electron distributions. Non-equilibrium distributions were observed for the first time by Fann et al. [15,16] and more recently by Lisowski et al. [17–19].

2 The model

The theoretical model is based on a simplified metal description, supposed perfect, homogeneous and isotropic. The electron conduction band is assumed parabolic and isotropic and the phonon dispersion relation well described by the Debye model [41]. The metal is considered thicker than the laser pulse absorption depth, so that the perturbation can be considered spatially homogeneous. Moreover, energy transport and diffusion effects have been neglected. Consequently, the model can be considered spatially homogeneous and isotropic, depending only on time and energy.

The model consists in solving the Boltzmann equation for electrons and phonons, considering the Fermi-Dirac and Bose-Einstein statistics, respectively.

The laser pulse is absorbed inducing energy jumps equal to the photon energy, adding a source term to the electron Boltzmann equation.

For the electron Boltzmann equation, the contribution of $e-e$ and $e-p$ collisions is considered, while, for the phonon Boltzmann equation, only $e-p$ collisions are included, neglecting photon-phonon and phonon-phonon interactions.

The system of the two-coupled Boltzmann equations assumes the following form:

$$\begin{aligned}\frac{\partial f(k,t)}{\partial t} &= \left.\frac{\partial f(k,t)}{\partial t}\right|_{ee} + \left.\frac{\partial f(k,t)}{\partial t}\right|_{ep} + \Phi \\ \frac{\partial N(q,t)}{\partial t} &= \left.\frac{\partial N(q,t)}{\partial t}\right|_{ep}\end{aligned} \tag{1}$$

where $f(k,t)$ and $N(q,t)$ represent the electron and phonon distribution functions, which, under our assumptions, depend only on the modulus of the momentum $\mathbf{k}$ and $\mathbf{q}$, respectively; Φ is the laser absorption source term, $\left.\frac{\partial f(k,t)}{\partial t}\right|_{ee}$ the $e-e$ collision integral, $\left.\frac{\partial f(k,t)}{\partial t}\right|_{ep}$ and $\left.\frac{\partial N(q,t)}{\partial t}\right|_{ep}$ the $e-p$ collision integrals for the electron and the phonon Boltzman equation, respectively.

2.1 Laser perturbation term

In noble metal films, the valence d-bands lie far below the conduction band. Considering laser photon energy ($h\nu$) lower than the interband transition threshold, the laser perturbation produces only intraband transition in the conduction band; laser photons are absorbed directly by conduction band electrons [3,4] through single-photon transition

$$e^-(E) + \gamma(h\nu) \rightarrow e^-(E + h\nu). \tag{2}$$

The electron population derivative in the energy state E is given by the differences of two terms, one corresponding to the loss of electrons with energy E excited toward higher levels and the other to the gain of electrons excited from lower levels

$$\begin{aligned}\frac{df_{exc}(E,t)}{dt} = \Delta\rho(t)\,\{&D(E-h\nu)f(E-h\nu)\,[1-f(E)] \\ &-D(E+h\nu)f(E)\,[1-f(E+h\nu)]\}\end{aligned} \tag{3}$$

being $D(E)$ the density of states. Equation (3) takes into account the Pauli exclusion principle by introducing the term $(1-f)$. The total number of conduction band electrons, given by

$$n_e = \int D_e(E) f(E,t) dE \tag{4}$$

must be conserved because of only intraband transitions are considered and the emitted electrons are neglected.

The factor $\Delta\rho\ (t)$ is proportional to the injected laser energy and to the pulse temporal profile and it is calculated considering the energy conservation:

$$\Delta\rho(t) = \frac{u_{abs}\lambda(t)}{\int ED(E)\frac{df_{exc}(E,t)}{dt}dE} \tag{5}$$

being u_{abs} the laser energy density (per unit volume) absorbed by the metal and $\lambda(t)$ the pulse temporal shape. Although the perturbed electron distribution is not a Fermi-Dirac, an equivalent excitation temperature T_{exc} can be associated, defined as the temperature of a Fermi-Dirac distribution with the same total energy as the perturbed distribution.

A crude estimation of T_{exc} can be obtained by the following approximate formula, based on a Fermi-Dirac statistics:

$$u_{abs} = \frac{1}{2}c_0\left(T_{exc}^2 - T_0^2\right) \Rightarrow T_{exc} = \left(T_0^2 + \frac{2u_{abs}}{c_0}\right)^{1/2} \tag{6}$$

where c_0 is electron specific heat and T_0 is the initial equilibrium temperature.

Calculations have been performed considering regimes in which the equivalent electron temperature ranges from few (2–3) to some hundreds (300) Kelvin above the metal temperature, which correspond to laser energy density absorbed per unit volume of $10^5\ \mathrm{J/m^3} \leqslant u_{abs} \leqslant 10^8\ \mathrm{J/m^3}$.

Laser absorbed energies must be lower than the damage threshold, to prevent phase transitions and lattice modification.

2.2 Electron-electron collisions

The interaction among conduction band electrons is a very complex multiparticle problem, but it can be simplified by introducing two important concepts, the quasi-particle and the screening concept [42,43].

To take into account the repulsion due to the other electrons, each electron could be described as surrounded by a positive charged cloud, whose effect is to screen out its electric potential at long distances. In this way, only electrons, which come very close, could interact each other. Thus, the electron surrounded by the positive charged cloud behaves as a new particle (quasi-particle), which interacts with the other quasi-particles through a screened potential. This interaction occurs on a short range and could be treated as a weak perturbation. The Landau's Fermi liquid theory could be then applied [42,43].

In the calculation of electron-electron scattering, only two-body scattering events have been considered. This approach of excluding three-body and many-body contributions will be valid as long as the average inter-particle spacing is large compared to the scattering radius, i.e., at low densities. Moreover, the many-body scatterings are characterized by a transition probability, which is negligible with not too strong laser perturbation.

The interaction between two quasi-particles can be considered as a two-body elastic collision in which total energy and momentum must be conserved.

In the calculation of $e-e$ collision integrals, only normal processes in which the momentum conservation occurs in the same cell of the reciprocal lattice will be considered and both umklapp processes [44,45] and exchange terms [46,47], which derive from the indistinguibility of the electrons, have been neglected.

In the first order perturbation theory framework, using the Fermi's golden rule, the probability that two electrons with wavevectors $\mathbf{k}_1$, $\mathbf{k}_2$ scatter into $\mathbf{k}_3$, $\mathbf{k}_4$ can be written as [48,49]:

$$\begin{aligned} S(\mathbf{k}_1,\mathbf{k}_2;\mathbf{k}_3,\mathbf{k}_4) = \frac{2\pi}{\hbar}\left|M_{ee}\right|^2\delta(\mathbf{k}_1+\mathbf{k}_2-\mathbf{k}_3-\mathbf{k}_4) \\ \times\delta(E_1+E_2-E_3-E_4)f(\mathbf{k}_1)f(\mathbf{k}_2)\left[1-f(\mathbf{k}_3)\right]\left[1-f(\mathbf{k}_4)\right] \end{aligned} \tag{7}$$

where the momentum and energy conservation conditions appear, together with Pauli's exclusion principle, $f(\mathbf{k}_1)f(\mathbf{k}_2)\left[1-f(\mathbf{k}_3)\right]\left[1-f(\mathbf{k}_4)\right]$, which takes into account the probability that the $\mathbf{k}_1$ and $\mathbf{k}_2$ states are occupied while the $\mathbf{k}_3$ and $\mathbf{k}_4$ are empty. The term M_{ee} represents the interaction matrix element, which is calculated from the $e-e$ interaction Hamiltonian, H_{ee}, through the following

$$M_{ee} = M_{ee}(\mathbf{k}_1,\mathbf{k}_2;\mathbf{k}_3,\mathbf{k}_4) = \left\langle \mathbf{k}_3,\mathbf{k}_4\left|H_{ee}\right|\mathbf{k}_1,\mathbf{k}_2\right\rangle. \tag{8}$$

The electron distribution change rate in the state $\mathbf{k}_1$ is given by the difference between the total scattering rate *into*, $\Gamma_{in}(\mathbf{k}_1)$, and *out*, $\Gamma_{out}(\mathbf{k}_1)$, from the state $\mathbf{k}_1$, respectively:

$$\begin{aligned} \left.\frac{df(k_1)}{dt}\right|_{ee} &= \Gamma_{in}(\mathbf{k}_1) - \Gamma_{out}(\mathbf{k}_1) \\ &= \frac{2\pi}{\hbar}\sum_{\mathbf{k}_2,\mathbf{k}_3,\mathbf{k}_4}\left|M_{ee}\right|^2 F(\mathbf{k}_1,\mathbf{k}_2,\mathbf{k}_3,\mathbf{k}_4) \\ &\quad\times\delta(\mathbf{k}_1+\mathbf{k}_2-\mathbf{k}_3-\mathbf{k}_4)\delta(E_1+E_2-E_3-E_4) \end{aligned} \tag{9}$$

where

$$\begin{aligned} F(\mathbf{k}_1,\mathbf{k}_2,\mathbf{k}_3,\mathbf{k}_4) = &-f(\mathbf{k}_1)f(\mathbf{k}_2)\left[1-f(\mathbf{k}_3)\right]\left[1-f(\mathbf{k}_4)\right] \\ &+\left[1-f(\mathbf{k}_1)\right]\left[1-f(\mathbf{k}_2)\right]f(\mathbf{k}_3)f(\mathbf{k}_4). \end{aligned} \tag{10}$$

The $e-e$ collision integral, given in equation (9), corresponds to the sum over all possible two-body scattering events in three dimensions, which populate and depopulate the state $\mathbf{k}_1$.

In the Thomas-Fermi theory approximation of a static electron screening, the screened Coulomb potential between any two electrons can be written in the following form:

$$H_{ee}^{screened} = \frac{e^2}{4\pi\varepsilon_0}\frac{1}{|\mathbf{r}_1-\mathbf{r}_2|}\exp\left[-q_s\left|\mathbf{r}_1-\mathbf{r}_2\right|\right] \tag{11}$$

where e is the electron charge, ε_0 the dielectric constant in void, $\mathbf{r}_1$ and $\mathbf{r}_2$ the electron positions and q_s the screening parameter. As shown in equation (11), the potential is

characterized by an exponential damping factor that reduces it to a negligible size at distances longer than $1/q_s$. The Thomas-Fermi theory screening parameter estimation (q_{TF}) is

$$q_{TF}^2 = \frac{e^2}{\varepsilon_0}\frac{\partial n_0}{\partial \mu} \tag{12}$$

where μ is the chemical potential and n_0 is the electron density. For a free electron gas, when $T \ll T_F$, where T_F is the Fermi temperature, $\frac{\partial n_0}{\partial \mu}$ is simply the density of levels at the Fermi energy, $D(E_F) = \frac{mk_F}{\hbar^2\pi^2}$, where m is the electron mass and k_F the Fermi vector. Therefore

$$q_{TF}^2 = \frac{e^2}{\varepsilon_0} D(E_F) = \frac{e^2 m k_F}{\varepsilon_0 \hbar^2 \pi^2}. \tag{13}$$

Using this estimation, we obtain a value of q_{TF} of the order of k_F; i.e., disturbances are screened at a distance, which is similar to the inter-particle spacing. Thus electrons are highly effective in shielding external charges. The screening in metals is very strong and $e-e$ interactions are considerably reduced. Moreover, as we will see, the $e-e$ scattering rate is very sensible to the value of the used screening parameter.

The $e-e$ matrix element $|M_{ee}|^2$ can be calculated from the screening Coulomb potential of equation (11). After different mathematical rearrangements, this quantity can be written as

$$|M_{ee}(\mathbf{q})|^2 = \left[\frac{e^2}{\varepsilon_0 V}\frac{1}{q^2+q_s^2}\right]^2 \tag{14}$$

and depends only on the scattering transferred momentum $\mathbf{q} = \mathbf{k}_1 - \mathbf{k}_3$.

If we pass to the continuous, the sums in equation (9) over the three possible values of $\mathbf{k}_2$, $\mathbf{k}_3$, $\mathbf{k}_4$ become an integral over 12 momentum dimensions. Under the hypothesis of a parabolic and isotropic conduction band ($E = \frac{\hbar^2 k^2}{2m}$), this integral can be expressed only in terms of electron energy and easily calculated. If E_1, E_2, E_3 and E_4 represent the electron energies corresponding to the momentum states $\mathbf{k}_1$, $\mathbf{k}_2$, $\mathbf{k}_3$ and $\mathbf{k}_4$, the collision integral for the state with electron energy E_1 and momentum state $\mathbf{k}_1$can be reduced analytically to a double integral over the electron energies E_2 and E_3 [5,48,49]. The final expression for the $e-e$ collision integral is thus:

$$\begin{aligned}\left.\frac{df(E_1)}{dt}\right|_{ee} dE_1 &= \Gamma_{in}(E_1) - \Gamma_{out}(E_1)\\ &= \frac{m^{5/2}}{2^{5/2}\pi^3\hbar^6}\frac{1}{\sqrt{E_1}}\frac{Se^4}{\varepsilon^2} dE_1 \iint dE_2 dE_3\\ &\quad\times\left[\frac{q}{2q_s^2(q^2+q_s^2)} + \frac{1}{2q_s^2}\arctan g\left(\frac{q}{q_s}\right)\right]\Bigg|_{q_{\min}}^{q_{\max}}\\ &\quad\times\{f(E_3)f(E_4)[1-f(E_1)][1-f(E_2)]\\ &\quad -f(E_1)f(E_2)[1-f(E_3)][1-f(E_4)]\}|_{E_4=E_1+E_2-E_3}\end{aligned} \tag{15}$$

where S is a spin factor (=2), ε the dielectric constant, and q_{max} and q_{min} are given by

$$\begin{cases} q_{\max} = \min\{(k_2+k_4);(k_1+k_3)\} \\ q_{\min} = \max\{|k_2-k_4|;|k_1-k_3|\}\end{cases}. \tag{16}$$

As we can see, the collision integral in equation (15) depends on the electron distribution so that $e-e$ scattering is a non-linear problem.

An estimation of $e-e$ relaxation times can be obtained through the Fermi-liquid theory (FLT) [41–43]. According to this theory, an electron of energy E_1 near the Fermi surface has a scattering rate $1/\tau$ that depends on its energy and temperature in the form

$$\frac{1}{\tau_{ee}} = a(E_1 - E_F)^2 + b(k_B T)^2 \tag{17}$$

where the coefficients a and b are independent of E_1 and T. Thus the electronic lifetime due to $e-e$ scattering can be made as large as one wishes by going to sufficiently low temperatures and considering electrons sufficiently close to the Fermi surface.

For electronic levels i such that $(E_i - E_F) \gg k_B T$, the leading contribution to the scattering rate $1/\tau_{ee}$ in equation (17) is the first term. In this case, the distribution thermal broadening plays no role and τ_{ee} does not depend on T. The thermal behaviour of the system prevails for electronic levels for which $(E_i - E_F) \ll k_B T$. In this last case, the elementary excitations lie within a layer of width $k_B T$ around the Fermi surface and their τ_{ee} are then nearly independent on E_i and proportional to T^{-2}. It gives qualitative measures of the collision time of a thermal excitation. Equation (17), however, no longer holds when $(E_i - E_F) \approx E_F$, thus this estimation of $e-e$ relaxation times holds only for electrons not too far from the Fermi energy.

2.3 Electron-phonon collisions

The $e-p$ interaction consists in phonon emission and absorption processes by the electron gas. In noble metals, such as Ag, only acoustic phonons, characterized by one longitudinal and two transverse modes, are present. Assuming that these phonon modes are distinct and considering only normal processes, in which the momentum conservation occurs in the same reciprocal lattice cell, only the longitudinal phonon acoustic mode is coupled to the electron gas [50]. This phonon mode is described by the Debye dispersion relation.

The phonon emission and absorption scattering process rates can be calculated through the Fermi's golden rule, in the framework of the first order perturbation theory [51].

The probability that an electron in the state $\mathbf{k}$ emits a phonon with wave number $\mathbf{q}$ and energy $E_\mathbf{q} = \hbar\Omega_\mathbf{q}$, scattering into the state $\mathbf{k}' = \mathbf{k} - \mathbf{q}$ is given by:

$$\begin{aligned}S(\mathbf{k};\mathbf{k}',\mathbf{q}) = \frac{2\pi}{\hbar}\Omega_{ep}(\mathbf{k}',\mathbf{q};\mathbf{k}) f(\mathbf{k})[1-f(\mathbf{k}')]\\ \times(1+N_\mathbf{q})\delta(E(\mathbf{k}) - E(\mathbf{k}') - \hbar\Omega_\mathbf{q})\end{aligned} \tag{18}$$

where $\Omega_{ep}(\mathbf{k}',\mathbf{q};\mathbf{k}) = |\langle\mathbf{k}',\mathbf{q}|\, H_{ep}\,|\mathbf{k}\rangle|^2$ represents the $e-p$ matrix element, with H_{ep} the $e-p$ interaction perturbation potential; $f(\mathbf{k})$ and N_q represent, respectively,

the electron and the phonon distribution function, corresponding to $\mathbf{k}$ and $\mathbf{q}$ wave vector; $f(\mathbf{k})\left[1-f(\mathbf{k}')\right](1+N_{\mathbf{q}})$ is the factor which takes into account the Pauli exclusion principle, since electron can scatter only into unoccupied states $[1-f(\mathbf{k}')]$, and the proportionality of the phonon emission processes on the factor $(1+N_q)$, since both spontaneous and stimulated emission should be included; and finally $\delta(E(\mathbf{k})-E(\mathbf{k}')-\hbar\Omega_{\mathbf{q}})$ is the total energy conservation condition. In the case of the inverse process of phonon absorption, the phonon absorption probability is proportional to N_q instead of $(1+N_q)$.

The electron distribution change in the state $\mathbf{k}$ due to $e-p$ collisions is given by the sum of two terms representing the total scattering rate of both phonon emission and absorption processes, involving transition towards all the states $\mathbf{k}'$ with $\mathbf{k}'=\mathbf{k}-\mathbf{q}<\mathbf{k}$ and $\mathbf{k}'=\mathbf{k}+\mathbf{q}>\mathbf{k}$ and considering all the possible phonon wave vectors in the first Brillouin zone:

$$\begin{aligned}\left.\frac{df(\mathbf{k})}{dt}\right|_{ep} &= \Gamma^{-}(\mathbf{k})+\Gamma^{+}(\mathbf{k})\\ &= \frac{2\pi}{\hbar}\sum_{\mathbf{q}}|M_{ep}|^2\left\{f(\mathbf{k}')\left[1-f(\mathbf{k})\right]N_{\mathbf{q}}-f(\mathbf{k})\left[1-f(\mathbf{k}')\right]\right.\\ &\times(1+N_{\mathbf{q}})\left.\right\}\delta(E(\mathbf{k})-E(\mathbf{k}')-\hbar\Omega_{\mathbf{q}})\\ &+\frac{2\pi}{\hbar}\sum_{\mathbf{q}}|M_{ep}|^2\left\{f(\mathbf{k}')\left[1-f(\mathbf{k})\right](1+N_{\mathbf{q}})-f(\mathbf{k})\right.\\ &\times\left[1-f(\mathbf{k}')\right]N_{\mathbf{q}}\left.\right\}\delta(E(\mathbf{k})-E(\mathbf{k}')+\hbar\Omega_{\mathbf{q}}).\end{aligned}\tag{19}$$

The corresponding phonon distribution changes are:

$$\begin{aligned}\left.\frac{dN(\mathbf{q})}{dt}\right|_{ep} &= \left.\frac{dN_{\mathbf{q}}}{dt}\right|_{ep}=2\frac{2\pi}{\hbar}\sum_{\mathbf{k}}|M_{ep}|^2\left\{f(\mathbf{k})\left[1-f(\mathbf{k}')\right]\right.\\ &\times(1+N_{\mathbf{q}})-f(\mathbf{k}')\left[1-f(\mathbf{k})\right]N_{\mathbf{q}}\left.\right\}\delta\left(E(\mathbf{k}')-E(\mathbf{k})-\hbar\Omega_{\mathbf{q}}\right).\end{aligned}\tag{20}$$

The $e-p$ matrix element can be calculated taking into account the $e-p$ interaction screening due to the electron gas, which reduces $e-p$ interaction. In the approximation of a static screening and in the Thomas-Fermi theory framework, the $e-p$ interaction matrix can be written:

$$\left|M_{ep}^{screen}(q)\right|^2=\frac{1}{\varepsilon_0 V}\frac{e^2}{q^2+q_s^2}\frac{1}{2}\hbar\Omega_q=\frac{e^2\hbar c}{2\varepsilon_0 V}\frac{q}{q^2+q_s^2}.\tag{21}$$

2.4 Collision integrals conservation properties

In the calculation of $e-e$ and $e-p$ collision integrals, the following conservation properties must be imposed:

(1) electron density conservation in the electron conduction band

$$n_e=\int D_e(E_e)f(E_e)dE_e=\cos t \Rightarrow \frac{dn_e}{dt}=\int D_e(E_e)\frac{df(E_e)}{dt}dE_e=0;\tag{22}$$

(2) total energy density conservation

$$E_{tot}=\int E_e D_e(E_e)f(E_e)dE_e=\cos t\Rightarrow dE_{tot}=0;\tag{23}$$

(3) detailed balance principle, accordingly, at equilibrium, the probability of a direct process must be equal to its inverse, in such a way that, for $t\to\infty$, the local thermodynamic equilibrium is reached.

In Appendix A, more details are given about the way in which such conservation properties have been imposed.

3 Numerical model

To perform the numerical solution of the two coupled Boltzmann equation, the electron and phonon energy axes have been divided into constant energy intervals (N_e and N_p, respectively) and the electron and phonon Boltzmann equations (Eq. (1)) result in a system of $N_t=N_e+N_p$ coupled, nonlinear differential equations.

Using a matrix representation, this system can be written in the following way:

$$\begin{aligned}\frac{d\mathbf{f}(t)}{dt}&=\mathbf{M}(\mathbf{f})\mathbf{f}\\ \frac{d\mathbf{N}(t)}{dt}&=\Omega^{+}(\mathbf{N}+1)-\Omega^{-}\mathbf{N}\end{aligned}\tag{24}$$

where $\mathbf{f}$ and $\mathbf{N}$ represent, respectively, the electron and phonon distributions vectors, while $\mathbf{M}$, Ω^{+} and Ω^{-} the matrices which take into account all the discussed processes. Let us note that the $\mathbf{M}$ matrix depends on the electron distribution $\mathbf{f}$, while Ω^{+} and Ω^{-} are independent of $\mathbf{N}$.

This system of differential equations has been solved using the implicit Euler algorithm. In particular, for the electron distribution

$$\frac{\mathbf{f}(t+dt)-\mathbf{f}(t)}{dt}=\mathbf{M}(\mathbf{f}(t))\mathbf{f}(t+dt)\tag{25}$$

as a consequence, once the electron distribution $\mathbf{f}(t)$ is known, the electron distribution $\mathbf{f}(t+dt)$ at time $t+dt$ is obtained using

$$\left[\mathbf{I}-dt\mathbf{M}(\mathbf{f}(t))\right]\mathbf{f}(t+dt)=\mathbf{f}(t).\tag{26}$$

For the phonon distribution, instead, the following equation has been used

$$\frac{\mathbf{N}(t+dt)-\mathbf{N}(t)}{dt}=\Omega^{+}(\mathbf{N}(t)+1)-\Omega^{-}\mathbf{N}(t+dt)\tag{27}$$

thus the solution at time $t+dt$ is obtained from the solution at time t through

$$\mathbf{N}(t+dt)=\frac{\mathbf{N}(t)(1+dt\Omega^{+})+dt\Omega^{+}}{1+dt\Omega^{-}}.\tag{28}$$

To improve the stability and the efficiency of this algorithmic, a step-adapting method has been used [52]. This method has been applied only to the electron Boltzmann equation, since the electron kinetics is faster and needs smaller time steps than phonon kinetics.

4 Results and discussion

Let consider an Ag film subjected to a 20 fs laser pulse with 1.45 eV photon energy. The total laser energy density injected is 2.56×10^7 J/m^3, which is approximately equivalent to an instantaneous electron temperature rise of $\Delta T_{exc} = 500$ K. Before irradiation, the metal film is supposed in equilibrium at room temperature ($T_0 = 300$ K), thus, electrons and phonons are described, respectively, by a Fermi-Dirac and a Bose-Einstein distribution function at T_0. According to the laser energy injected and to the electron and phonon heat capacities, the expected final equilibrium temperature is $T_F = 330$ K. Both in $e-e$ and $e-p$ collision integrals, the screening parameter value of 5.5×10^9 m^{-1} has been used. This value has been chosen in such a way that the resulting $e-e$ relaxation times are comparable with experimental ones obtained with 2PPE experiments (see Sect. 4.7).

4.1 Electron distribution changes

Figure 1 shows the temporal evolution of the electron energy distribution function (eedf) versus electron energy, near and above the Fermi level E_F, (a) during ($t \leqslant 20$ fs) and (b) after ($t > 20$ fs) laser perturbation.

As we can see from Figure 1a, the laser perturbation effect on eedf is to create strong non-equilibrium distributions characterized by a step shape with the photon energy periodicity ($h\nu_{las} = 1.45$ eV). The first principal step in the distribution goes from the Fermi level ($E_F = 5.49$ eV) up to $E_F + h\nu_{las} = 6.94 \sim 7$ eV. This is due to the one-photon absorption process by the electrons with energies E in the energy range $[E_F - h\nu_{las}, E_F]$. Excited electrons, in turn, can absorb a further photon, leading to an occupation number increase for energies up to $2h\nu_{las}$ above E_F, thus creating the second step and so on. During laser perturbation, eedf keeps rising, maintaining the step shape. Already on fs time scale, $e-e$ collisions start affecting the distribution by faster smoothing the steps in the eedf distribution tail. This effect is due to the electron energy redistribution, which pushes the eedf toward the equilibrium Fermi-Dirac distribution. As shown in Section 4.7, $e-e$ characteristic relaxation times go from few femtoseconds for electrons far from the Fermi level to some hundreds of femtoseconds for electrons near the Fermi level. This explains how, for $t \leqslant 20$ fs, $e-e$ collisions affect especially higher energy electrons.

After laser perturbation (Fig. 1b), eedf stops rising and the step shape disappears. From now on, besides $e-e$ collisions, also the $e-p$ interaction effect starts becoming observable. $e-p$ collisions allow the energy exchange between the electron and the phonon gas, leading to the transfer of the electron energy excess, due to the laser perturbation, towards the phonon system. As a consequence, the electron gas cools down and the eedf tends to approach a Fermi-Dirac distribution at the final equilibrium temperature T_F. This occurs only after 3 ps.

As we can see from Figure 1b, also during the cooling, transient electron distributions differ appreciably by

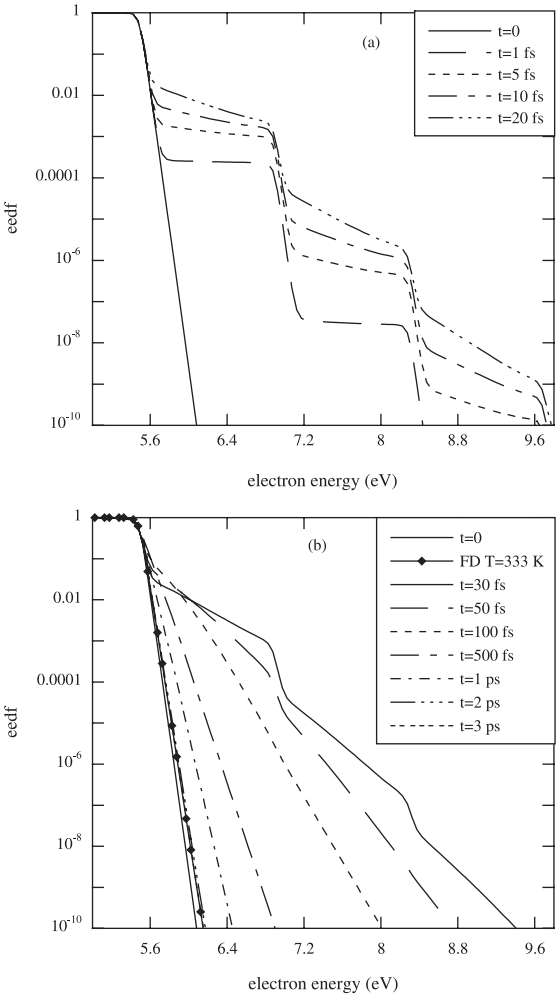

Fig. 1. Eedf time evolution for an Ag film under a 20 fs laser pulse with 1.45 eV photon energy and a total laser energy absorbed of 2.56×10^7 J/m^3 ($\Delta T_{exc} = 500$ K) (a) during and (b) after laser perturbation.

equilibrium Fermi-Dirac and an equilibrium temperature cannot be associated to these distributions. A confirm of this result can be obtaining by showing that any temperature definition attempts fail in describing the non-equilibrium electron behaviour. As an example, two different temperature definitions have been proposed: the first one, called T_{fit}, is obtained by fitting the electron distribution with a Fermi-Dirac distribution, while the second, called T_{exc}, is defined as the temperature of the Fermi-Dirac distribution which has the same internal energy of the non-equilibrium electron distribution. Figure 2 shows the comparison between the non-equilibrium electron distribution at the end of the laser pulse ($t = 20$ fs) and the Fermi-Dirac distributions at the two calculated temperatures T_{fit} (332 K) and T_{exc} (797 K) at the same instant. First of all, we can observe that, T_{fit} is only few tens of Kelvin degree higher than the initial equilibrium temperature $T_0 = 300$ K. This is due to the fact that the laser energy injected is transferred essentially to the eedf tail, which does not appreciably contribute to the calculation

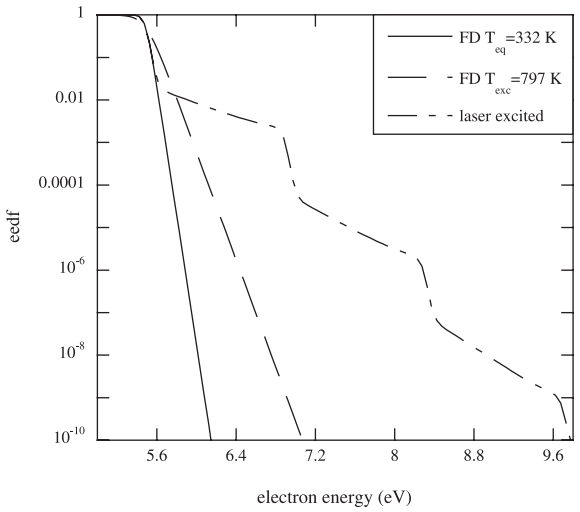

Fig. 2. Comparison between the non-equilibrium electron distribution at the end of the laser perturbation ($t = 20$ fs) and the Fermi-Dirac distributions at the two calculated temperatures $T_{fit} = 332$ K and $T_{exc} = 797$ K.

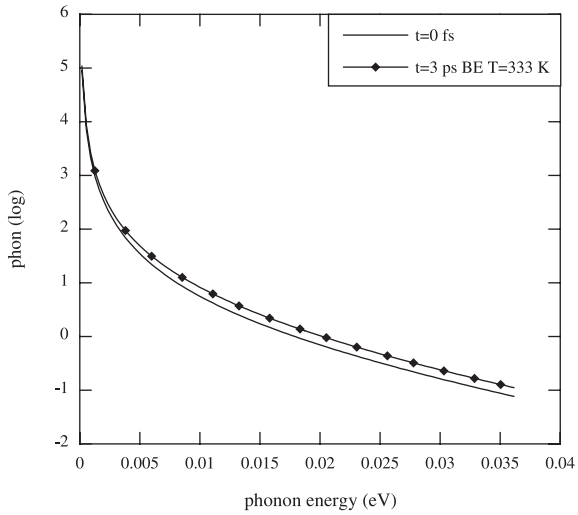

Fig. 3. Time evolution of the phonon distribution logarithmic for an Ag film under a 20 fs laser pulse with 1.45 eV photon energy and a total laser energy absorbed of 2.56×10^7 J/m^3 ($\Delta T_{exc} = 500$ K).

Table 1. T_{fit} and T_{exc} time evolution, corresponding to the electron distribution of Figure 1.

time	T_{fit}(K)	T_{exc}(K)
1 fs	300.41	346.27
5 fs	303.18	479.39
10 fs	309.38	604.82
20 fs	332.21	797.58
50 fs	421.27	786.16
100 fs	563.19	761.05
500 fs	622.44	564.51
1 ps	440.73	410.66
2 ps	340.83	331.28
3 ps	334.89	330.37

of T_{fit}. T_{fit} depends essentially on the population of the levels close to Fermi energy and it could describe relatively well only the low energy distribution. However, T_{fit} strongly underestimates the internal electron energy and badly describes the non-equilibrium behaviour of the eedf tail. To correctly describe the real internal electron energy, we can use T_{exc}, but, as we can see from Figure 2, also T_{exc} does not succeed to describe the non-equilibrium behaviour of the eedf tail. The corresponding T_{fit} and T_{exc} time evolution are reported in Table 1. It's clear that, during laser perturbation, T_{fit} remains more or less near the initial equilibrium temperature $T_0 = 300$ K, since laser energy is transferred essentially to the electron distribution tail, while T_{exc} increases up to the expected value of 800 K, since its value depends on the internal electron energy.

After the perturbation, T_{exc} decreases monotonically due to the $e-p$ energy transfer from electrons to phonons, while T_{fit} first increases up to 622 K ($t = 500$ fs) and then decreases. The T_{fit} increase is due to the higher excited electron relaxation towards lower energies due to $e-e$ collisions. The highest value reached by T_{fit} (622 K) is, however, smaller than the electron temperature rise expected (800 K), since for $t = 500$ fs, $e-p$ collisions have already transferred part of the excess electron energy toward the phonons.

4.2 Phonon distribution changes

Figure 3 reports the simultaneous phonon distribution time evolution in our test case. Phonon distribution changes are smaller and slower respect to eedf's ones. In the present model, phonons are not directly affected by laser perturbation, but they fell its effect only indirectly through the interaction with the electrons. This assumption is validated by the observation that phonon heat capacity is larger than the electron one, that's way laser perturbation is supposed to be absorbed only by the electron gas. As the eedf cools down, phonon distribution warms up and moves slightly and slowly towards the final equilibrium condition reached at $t = 3$ ps, attaining exactly a Bose-Einstein distribution at the final equilibrium temperature T_F.

Figure 4, instead, shows the phonon population time evolution corresponding to some phonon energy states ($E_q/E_q^{\max} = 0.40; 0.60; 0.80; 0.90$, where E_q is the phonon energy corresponding to a wave number q and $E_q^{\max}$ is the phonon energy corresponding to the maximum wave number q_{max} of the first Brillouin zone). Phonon population starts increasing after approximately some hundreds of femtoseconds ($t > 100$ fs), but phonon changes become more visible in the picosecond range.

Despite the fact that phonon distribution changes are much smaller than the electron ones, also phonon distribution passes through non-equilibrium states during its time evolution.

To prove this, let notice that, at equilibrium, $\left(\frac{dN_q}{dt}\right) = 0$ and, consequently, the following relation holds between

Table 2. Equilibrium values of the ratio Ω^+/Ω^- calculated by equation (29) corresponding to the two temperatures T_0 and T_F.

	$E_q/E_q^{\max} = 0.005$	$E_q/E_q^{\max} = 0.50$	$E_q/E_q^{\max} = 0.99$
$T_0 = 300$ K	0.992998399	0.491816819	0.24703649
$T_F = 333$ K	0.993632877	0.524591502	0.280520526

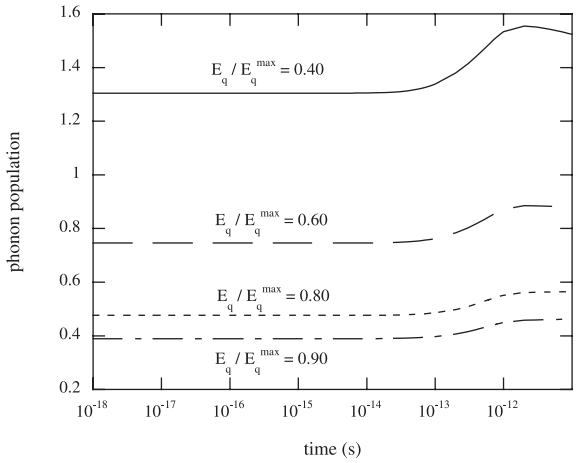

Fig. 4. Phonon population time evolution for different phonon energy states.

the total phonon emission Ω^+ and absorption rate Ω^- (Appendix A)

$$\frac{\Omega^+}{\Omega^-} = \frac{N_q}{N_q + 1} = e^{-\frac{E_q}{KT_p}} \tag{29}$$

where we have used for N_q a Bose-Einstein distribution at the phonon temperature T_p.

Figure 5 show the time evolution of the ratio Ω^+/Ω^- for phonons with energies (a) $E_q/E_q^{\max} = 0.005$, (b) $E_q/E_q^{\max} = 0.50$ and (c) $E_q/E_q^{\max} = 0.99$. Both at the beginning and at the end of the time evolution, when the phonon distribution is at equilibrium at $T_0 = 300$ K and $T_F = 333$ K, respectively, the values of the ratio Ω^+/Ω^- correspond exactly to those predicted by equation (29) at the two different temperatures. These values are reported in Table 2. However, in the between of equilibrium states, the ratio values are very far from equilibrium, showing the non-equilibrium of the phonon intermediate distributions.

4.3 Electron, phonon and total energy density time evolution

The internal energy density of the electron gas, $u_e(t)$, and the phonon gas, $u_p(t)$, can be calculated by integrating over the corresponding distribution functions, $f(E,t)$ and $N_q(E_q,t)$, taking into account both the electron and the phonon density of states, $D_e(E)$ and $D_p(E)$, respectively:

$$u_e(t) = \int dE_e D_e(E_e) E_e f(E_e)$$
$$u_p(t) = \int dE_q D_q(E_q) E_q N_q(E_q). \tag{30}$$

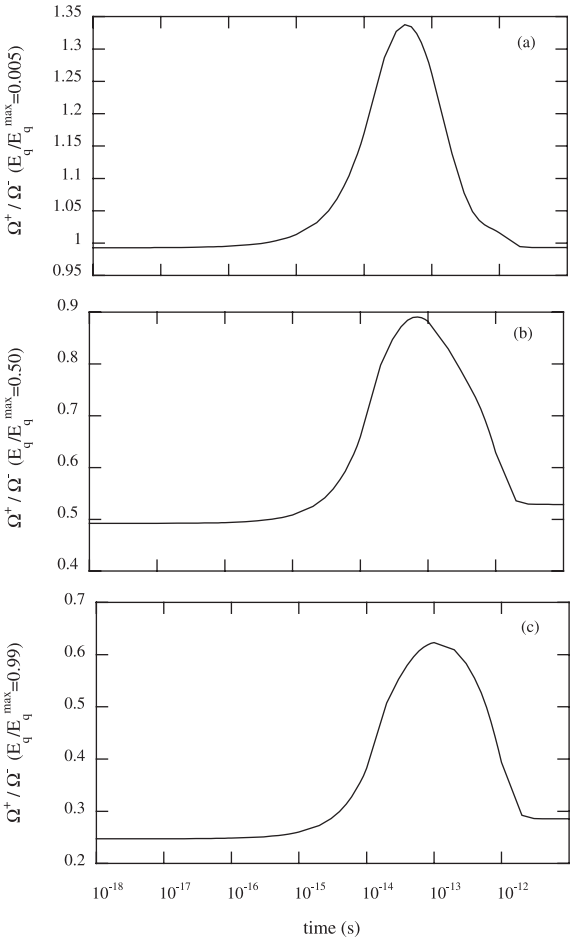

Fig. 5. Ω^+/Ω^- time evolution corresponding to energy phonon (a) $E_q/E_q^{\max} = 0.005$, (b) $E_q/E_q^{\max} = 0.50$ and (c) $E_q/E_q^{\max} = 0.99$, respectively.

Total energy density $u_{tot}(t)$, instead, is given by the sum:

$$u_{tot}(t) = u_e(t) + u_p(t). \tag{31}$$

Figures 6 and 7 show $u_e(t)$, u_p(t) and $u_{tot}(t)$ time evolution, corresponding to the electron and phonon distribution time evolution in Figures 1 and 3. During laser perturbation ($t \leqslant 20$ fs), $u_e(t)$ increases progressively, while $u_p(t)$ is nearly unaffected during the pulse. When the laser is turned off, $u_e(t)$ starts decreasing, while $u_p(t)$ increases, due to the $e-p$ electron energy transfer towards the phonons. Stationary $u_e(t)$ and $u_p(t)$ are achieved at $t = 3$ ps, when the new equilibrium condition is reached.

As shown in Figure 7, during laser perturbation, $u_{tot}(t)$ increases due the electron energy density increase, but, after the laser perturbation, it remains constant. This happens because both $e-e$ and $e-p$ collisions conserve total

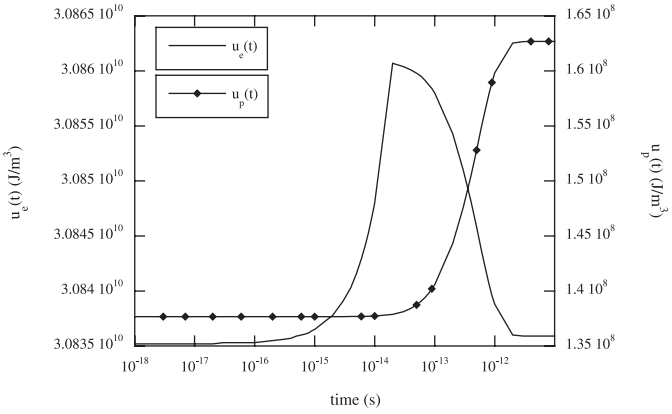

Fig. 6. Electron ($u_e(t)$) and phonon energy ($u_p(t)$) density time evolution corresponding to the electron and phonon distributions of Figures 1 and 3.

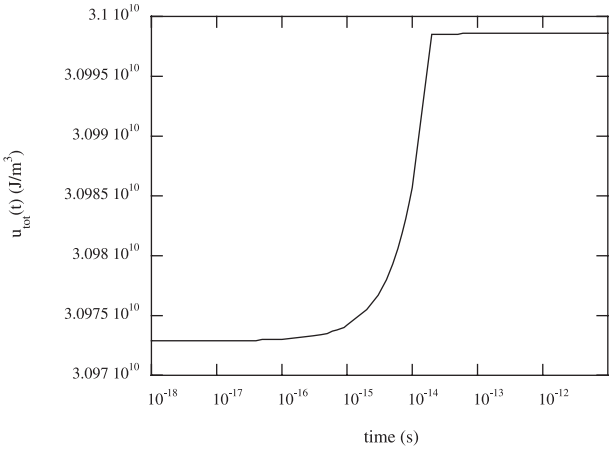

Fig. 7. Total energy density $u_{tot}(t) = u_e(t) + u_p(t)$ time evolution corresponding to the electron and phonon distribution time evolution of Figures 1 and 3.

energy. The total energy density conservation is a good check of the calculation numerical stability.

Besides the quantities $u_e(t)$, $u_p(t)$ and $u_{tot}(t)$, the electron, phonon and total energy density gain can be also calculated using

$$\begin{aligned} \delta u_e(t) &= u_e(t) - u_e(t=0) \\ \delta u_p(t) &= u_p(t) - u_p(t=0) \\ \delta u_{tot}(t) &= u_{tot}(t) - u_{tot}(t=0). \end{aligned} \tag{32}$$

Their time evolution is shown in Figure 8. During laser perturbation, δu_e increases following the increase of δu_{tot}. The latter, at the pulse end, reaches the expected value of 2.56×10^7 J/m^3, corresponding to the imposed total laser energy density injected. Moreover, during irradiation, phonon energy is nearly unaffected. Only after irradiation, thanks to $e-p$ collisions, the phonon gas is heated at the same rate as the electron gas is cooled. As a result, $\delta u_{tot}(t)$ remains constant after the laser perturbation.

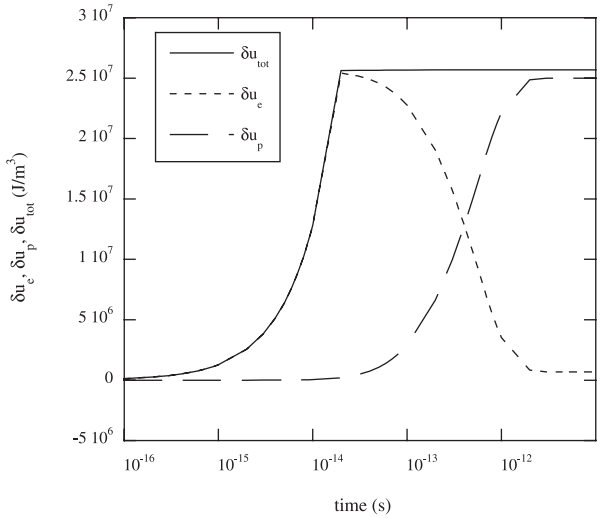

Fig. 8. Energy density increase time evolution of the electron gas, $\delta u_e(t)$, the phonon gas, $\delta u_p(t)$, and of the total energy, $\delta u_{tot}(t)$, for the test case considered (Ag, $dt_{las} = 20$ fs, $h\nu_{las} = 1.45$ eV, $u_{abs} = 2.56 \times 10^7$ J/m^3 ($\Delta T_{exc} = 500$ K)).

4.4 Comparison with TTM

Previous results have shown that the electron distribution function, after a femtosecond laser pulse excitation, can remain in non-equilibrium condition for some hundreds of femtoseconds up to the picosecond time scale. These results show the inadequacy of the TTM description for the electron and phonon relaxation dynamics in this temporal regime.

Two reasons for the TTM inadequacy can be outlined. The first is that $e-e$ collisions are not fast enough to thermalize the electron gas before the pulse end. Although high energies electrons are characterized by $e-e$ relaxation times of few femtoseconds (see 2PPE results in Sect. 4.7), electrons near the Fermi level have longer relaxation times due to available phase space absence.

Moreover, the TTM treats in a separate and sequential way $e-e$ and $e-p$ collisions. Figures 6 and 8 shows that when the laser is turned off, already for $t > 200$ fs, electron energy starts decreasing while phonon energy increases thanks to $e-p$ collisions. Therefore $e-p$ characteristic times start already at $t = 200$ fs up to few tens of picoseconds. As a consequence, $e-e$ and $e-p$ relaxation times overlap in a substantial temporal range so that separate and sequential treatment of the two kinds of collisions should be avoided.

Another confirm of TTM inadequacy can be obtained by comparing the $e-p$ cooling behaviour of the laser-excited electron gas with that of a Fermi-distributed electron gas with the same internal energy.

Figure 9 shows the corresponding time evolution of the transient internal excess energy in the following three cases in which the Ag film, initially in equilibrium at $T_0 = 300$ K, is subjected to a 100 fs laser pulse with the following laser energy density injected and excitation

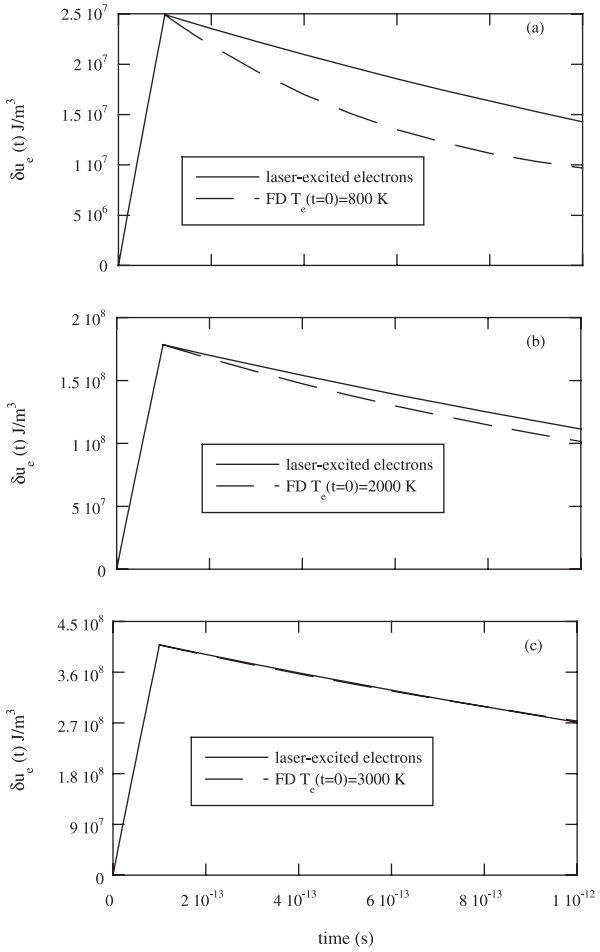

Fig. 9. Electron energy density increase time evolution $\delta u_e(t)$ (solid lines) for an Ag film subjected to a 100 fs laser pulse, with $h\nu_{las} = 1.45$ eV and a laser energy injected of (a) $u_{abs} = 2.56 \times 10^7$ J/m^3; (b) $u_{abs} = 1.83 \times 10^8$ J/m^3; (c) $u_{abs} = 4.08 \times 10^8$ J/m^3. The dashed lines show the cooling of the corresponding Fermi-distributed electron gas, which has the same internal energy at the time in which the laser perturbation is turned off ($t = 100$ fs).

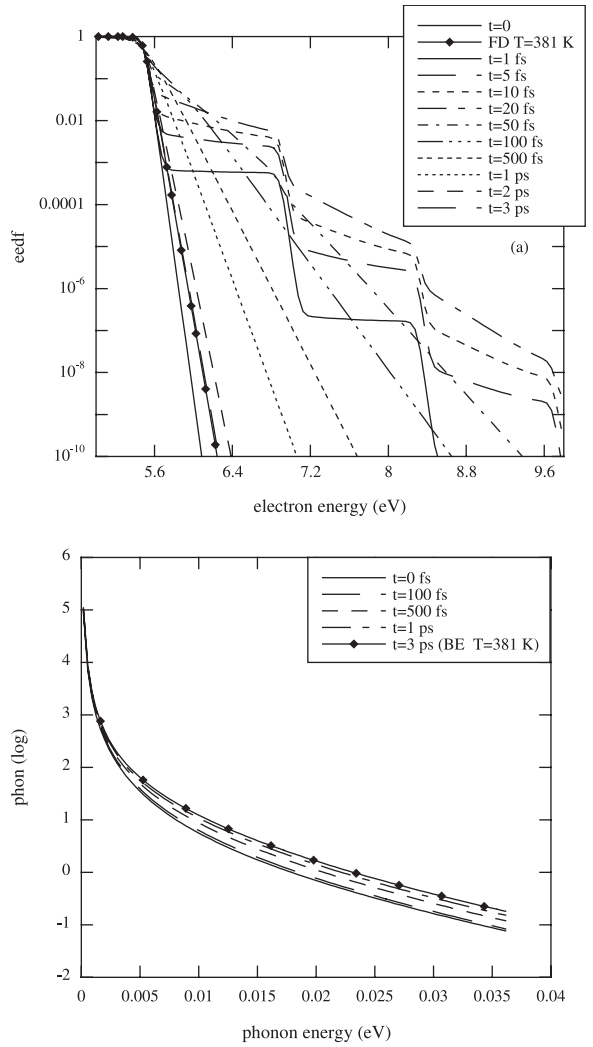

Fig. 10. (a) Electron distribution and (b) phonon distribution time evolution for an Ag film subjected to 20 fs laser pulse, with $h\nu_{las} = 1.45$ eV and with $u_{abs} = 6.30 \times 10^7$ J/m^3, i.e. $\Delta T_{exc} = 900$ K. The screening parameter used is $q_s = 5.5 \times 10^9$ m^{-1} and the $e - p$ matrix is given by equation (21).

temperatures:

a) $u_{abs} = 2.56 \times 10^7$ J/m^3, $T_{exc} = 800$ K
b) $u_{abs} = 1.83 \times 10^8$ J/m^3, $T_{exc} = 2000$ K
c) $u_{abs} = 4.08 \times 10^8$ J/m^3, $T_{exc} = 3000$ K.

In the calculations, only $e - p$ collisions have been considered. In the case of lower injected laser energies (Figs. 9a, 9b), the laser-heated electron gas cooling rate is slower than the Fermi-distributed electron gas one. This $e - p$ relaxation delay compared with the TTM prediction has been also theoretically [10] and experimentally observed [6,29,36]. Thus, for small injected laser energy, the non-equilibrium electron distribution slows down $e-p$ collisions.

However, Figure 9 shows also that by increasing the injected laser energy, the two cooling behaviours become closer and closer, up to coincide. This result shows that, in general, for large laser energy injected, the electron gas cooling behaviour depends only on the internal energy $u_e(t)$ and not on the particular electron distribution features. As a result, if sufficiently high laser energy is injected into the metal, the TTM prediction are fairly good to describe the electron cooling behaviour, also when a femtosecond laser pulse is used. For an explanation of this effect, the reader can refer to reference [10].

4.5 Different energy laser density excitations

In this section, the effect of laser energy density increase on electron and phonon relaxation dynamics is studied. Figure 10 shows the electron (a) and phonon (b) distribution time evolution in the case in which the Ag film is subjected to a higher laser energy density of $u_{abs} = 6.30 \times 10^7$ J/m^3 corresponding to $\Delta T_{exc} = 900$ K. The final equilibrium temperature expected is 381 K.

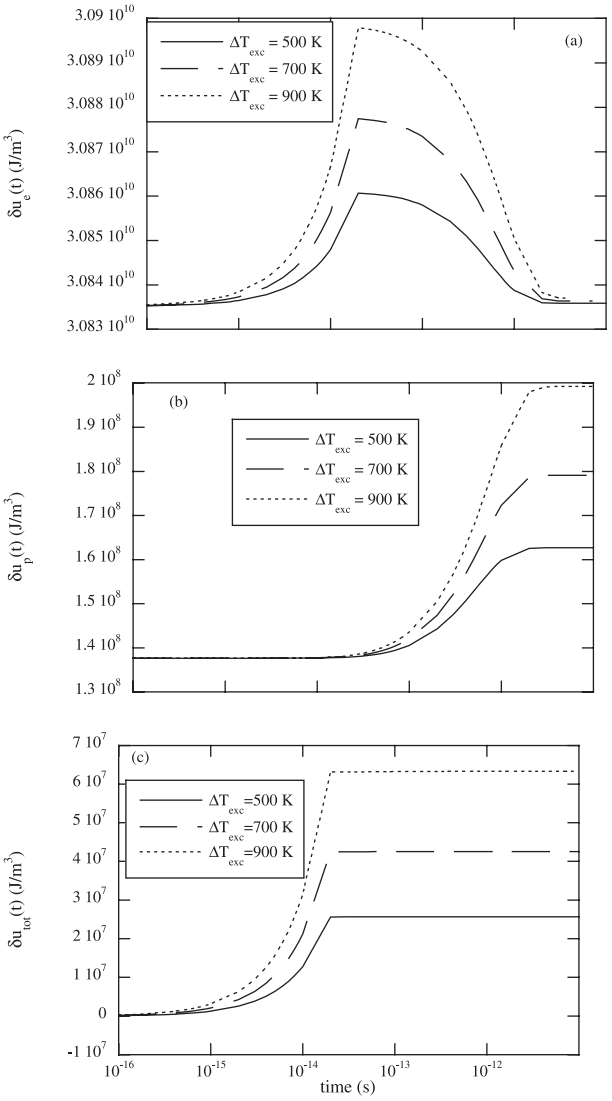

Fig. 11. Comparison of the (a) electron energy increase, $\delta u_e(t)$, (b) phonon energy increase, $\delta u_p(t)$, and (c) total energy increase $\delta u_{tot}(t)$ time evolution, in the three excitation cases considered (ΔT_{exc} = 500, 700 and 900 K).

Increasing the laser energy density leads to the increase of the fraction of electrons, which, from energies lower than E_F, are excited towards upper levels. As a consequence, for energies greater than E_F, higher plateaus in the electron distribution are observed (compare Figs. 1a and 10a).

Figure 11, instead, shows the comparison of (a) the electron energy increase, $\delta u_e(t)$, (b) the phonon energy increase, $\delta u_p(t)$, and (c) the total energy increase $\delta u_{tot}(t)$, in three excitation cases corresponding to ΔT_{exc} = 500, 700 and 900 K. As shown in Figure 11, the global relaxation time does not change with the increase of laser energy density.

However, the $e-p$ electron cooling and phonon heating rate become faster for higher laser excitations (see Fig. 11). $e-p$ collision rate depends essentially on the difference between the electron and phonon internal energy density. The greater the laser energy absorbed by the electron gas, the higher the difference between the electron and phonon internal energy density, the faster the $e-p$ energy transfer.

4.6 Different laser duration pulses

In this section, the role of the laser pulse duration keeping constant the absorbed energy is studied. Calculations have been performed in the same condition as in the test case corresponding to ΔT_{exc} = 500 K, but for different laser pulse durations dt_{las}.

Figure 12 shows the electron distribution time evolution for (a) dt_{las} = 0 s (instantaneous perturbation), (b) dt_{las} = 50 s, (c) dt_{las} = 400 fs and (d) dt_{las} = 1 ps. First of all, the pulse duration has no consequences over the electron distribution global relaxation times. As a matter of fact, in all the previous cases, the final equilibrium condition is reached at t = 3 ps.

However, comparing these figures, we can note that the electron distribution shape strongly depends on the laser pulse duration. Moreover, passing from the instantaneous excitation to a 1 ps laser pulse, the electron distribution step shape is washed out and the characteristic non-equilibrium structure is reduced. This happens because for longer dt_{las}, $e-e$ and $e-p$ collision processes have enough time to affect the distributions and to reduce the non-equilibrium effects before the laser pulse end.

This is also shown in Figure 13, where we compare the electron distribution shape corresponding to the perturbation last instant ($t = dt_{las}$) with different dt_{las}. For dt_{las} of some ten of femtoseconds (for example, for dt_{las} = 50 fs), the laser absorption steps are rounded off essentially by $e-e$ collisions. This effect is more visible in the distribution tail, which corresponds to electrons characterized by shorter $e-e$ relaxation times. For dt_{las} of some hundreds of femtoseconds ($dt_{las} > 200$ fs), instead, also $e-p$ collisions contribute in reducing the laser absorption steps. As a consequence, when the laser pulse is turned off, the electron distribution has been already relaxing towards the final equilibrium temperature.

These results can justify the use of the TTM in the description of the electron and phonon relaxation dynamic when a picosecond laser pulse is used: in this case, the electron distribution at the laser perturbation end can be considered more or less "thermalized".

In Figure 14 the electron, phonon and total energy density increase time evolution for the cases (a) dt_{las} = 50 fs, (b) dt_{las} = 200 fs, (c) dt_{las} = 400 fs and (d) dt_{las} = 1 ps are shown. By increasing the laser pulse duration, the electron energy density increase starts deviating from the total energy increase, since part of the electron energy is already transferred to the phonon gas.

Finally, in Figure 15, the electron and phonon energy time evolution are compared for dt_{las} in the range [10 fs–50 fs] (Figs. 15a and 15b) and [100 fs–2 ps] (Figs. 15c and 15d).

Observing Figures 15a and 15b, after the perturbation, electron cooling and phonon heating times do not change

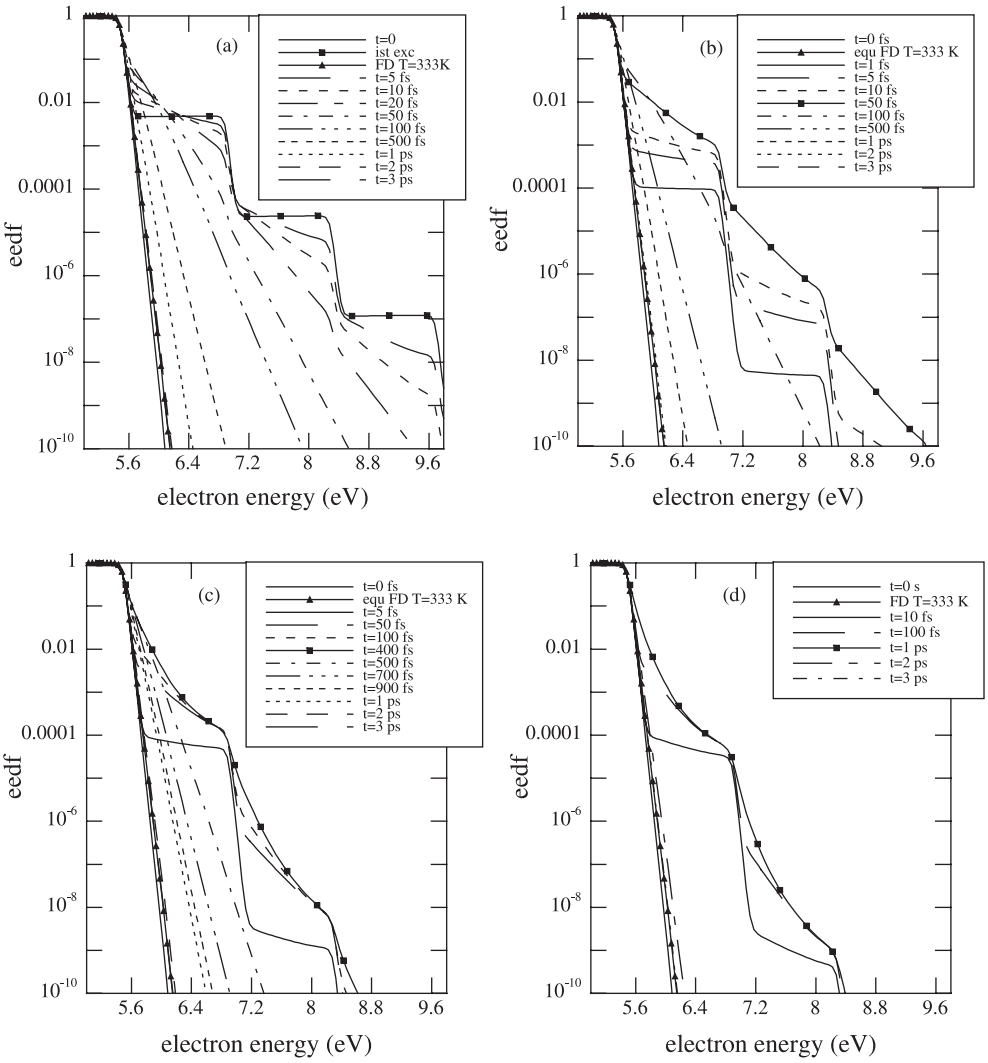

Fig. 12. Electron distribution time evolution (Ag film, $h\nu_{las} = 1.45$ eV and $\Delta T_{exc} = 500$ K) corresponding to different laser pulse durations: (a) instantaneous excitation; (b) $dt_{las} = 50$ fs; (c) $dt_{las} = 400$ fs and (d) $dt_{las} = 1$ ps.

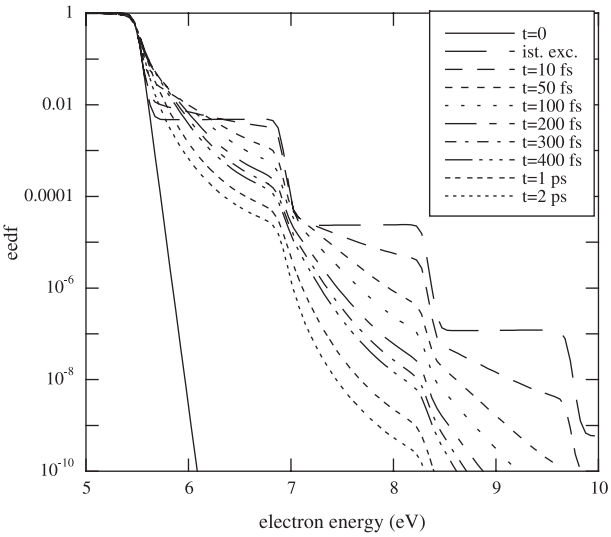

Fig. 13. Electron distribution at the end of laser perturbation ($t = dt_{las}$) for different dt_{las}.

when dt_{las} varies in the range [10 fs–50 fs]. On the contrary, (Figs. 15c and 15d), for dt_{las} in the range [100 fs–2 ps], the longer the laser pulse the slower the electron cooling and the phonon heating processes.

This phenomenon can be explained by considering that $e-p$ global collision times depend essentially on the electron and phonon internal energy density difference. The greater this difference, the smaller $e-p$ collision times. By increasing the dt_{las} in the range [100 fs–2 ps], an increasing laser energy fraction is transferred to the phonon subsystems due to $e-p$ collisions. As a consequence, the increase of dt_{las} in this range results in a smaller difference between the internal electron and phonon energies.

4.7 Comparison with 2PPE

Time-resolved two-photon photoemission experiments (2PPE) directly measure both the electron distribution function relaxation and the $e-e$ relaxation times as a function of the electron energy.

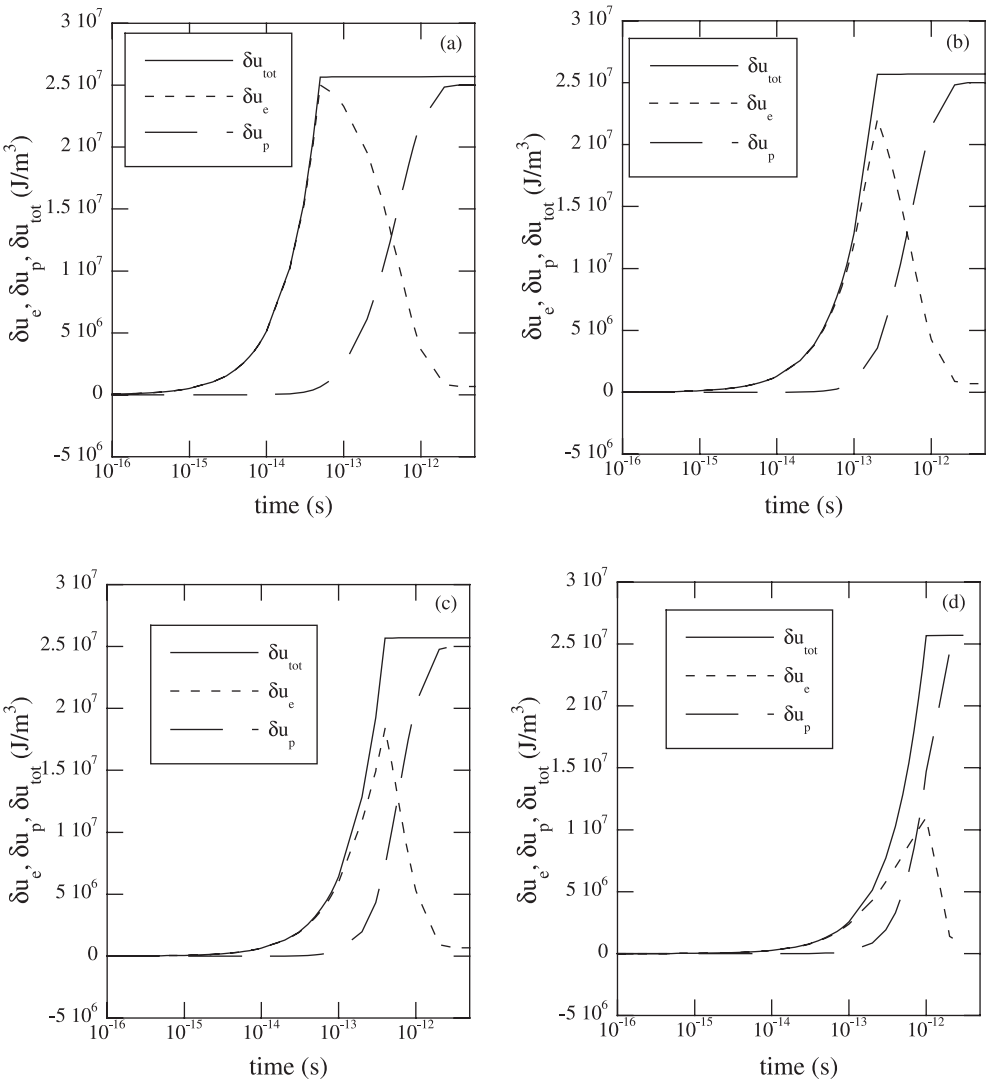

Fig. 14. Time evolution of energy increase for the electron gas, $\delta u_e(t)$, the phonon gas, $\delta u_p(t)$ and the total energy $\delta u_{tot}(t)$ in the cases (a) dt_{las} = 50 fs, (b) dt_{las} = 200 fs, (c) dt_{las} = 400 fs and (d) dt_{las} = 1 ps.

2PPE experiments consist in a pump-and-probe experiments, in which the first pulse excite electrons below the Fermi level E_F towards normally unoccupied states, while the second pulse photo-ionizes such excited electrons. By monitoring the number of photoelectrons as a function of the two pulse time delay and the corresponding kinetic energy, a direct measure of the electron distribution relaxation and of the intermediate state lifetimes can be determined. When femtosecond laser pulses are used, this technique is able to measure lifetimes of one or two femtoseconds. On this time scale, the measured lifetimes are due to $e-e$ relaxation times. $e-p$ scattering becomes important when relaxation times increase beyond some hundreds of femtoseconds ($t > 100$ fs). Moreover, since phonon energies are only few meV for typical metals, the energy loss due to phonon creation is too small to be resolved by energy analyzer commonly used in 2PPE experiments [19].

As an example, in reference [17], 2PPE experiment has been used to study the non-equilibrium electron and hole distributions dynamics of bare and D_2O covered ruthenium (Ru (001)) following optical excitation (55 fs, 800 nm pulses) with variable fluence (0.04–0.6 mJcm^{-2}).

These 2PPE spectra show very similar behaviour to our calculated electron distributions, although the material and the laser characteristic considered are different. As a matter of fact, similar plateaux in the electron range $E - E_F = h\nu_{las}$ and similar relaxation dynamics are observed, although different thermalization times occur. In Ru, the thermalization is faster (500 fs) than noble metals.

In reference [17], 2PPE spectra have been monitored also changing laser fluence. By increasing laser fluence, an increase of the non-equilibrium electrons relative number occurs and higher plateau in the range $E-E_F = h\nu_{las}$ appear. This behaviour has been found also in our calculated distributions (see Sect. 4.5).

Concerning $e-e$ lifetimes of individual excited electron states, Figure 16 shows the experimental electron state lifetimes τ_{PE} (fs) versus the electron energy $E - E_F$ obtained in 2PPE experiments for an Ag film (Refs. [20–22]). In this picture, the $e-e$ relaxation times theoretical prediction by the Fermi liquid theory (FLT) (see Eq. (17)) is also reported. As clearly shown, characteristic $e-e$

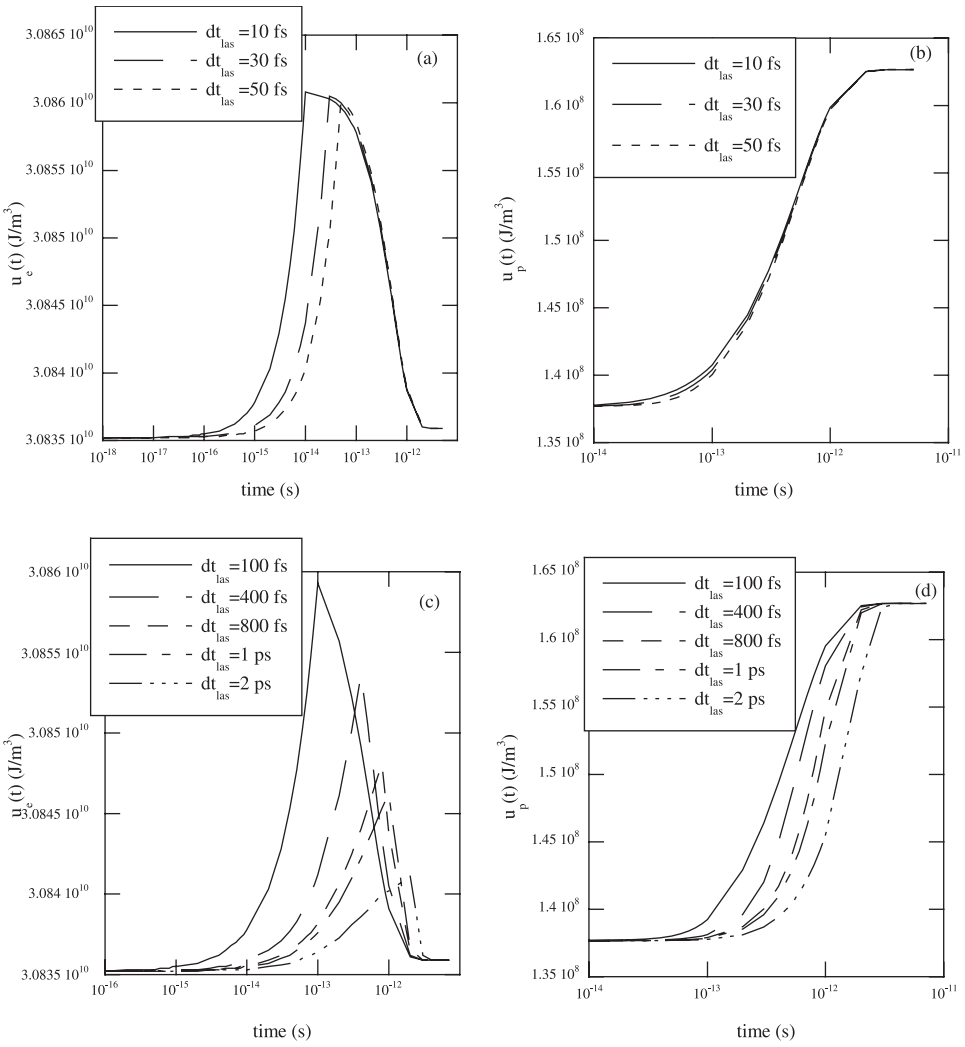

Fig. 15. Electron ((a) and (c)) and phonon ((b) and (d)) energy time evolution for different dt_{las}. (a) and (b) correspond to the range [10 fs–50 fs], while (c) and (d) to the range [100 fs–2 ps].

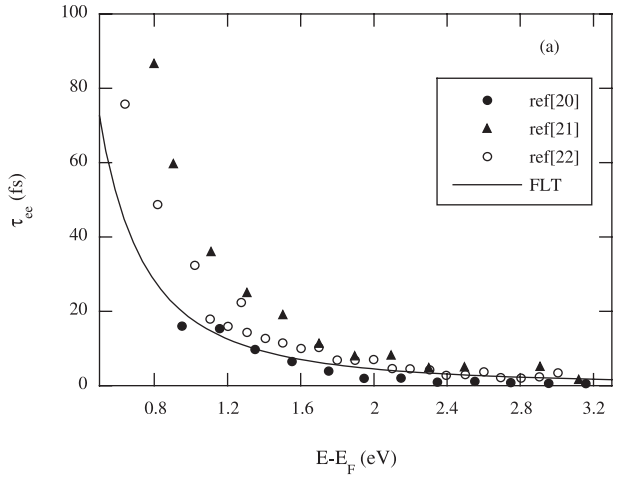

Fig. 16. Measured lifetimes τ_{PE} (fs) versus $E - E_F$ in 2PPE experiments for an Ag film (filled circle [20], filled triangle [21], open circle [22]) The solid line is calculated from Fermi liquid theory.

relaxation times go from few femtoseconds for electron levels with $(E - E_F) \approx 3$ eV to several tens of femtoseconds for $E - E_F$ less than 1.6 eV up to hundreds of femtoseconds for electrons very near to the Fermi level. Moreover, we note that experimental values calculated for Ag from references [20–22] give comparable results only for $E - E_F$ greater than 1.6 eV. For $E - E_F$ less than 1.6 eV, big differences are present. This depends on cascade effects, which make the 2PPE experimental technique less accurate for energies nearer to the Fermi level. As a matter of fact, the population of a state may be filled due to the energetic decay of higher excited electrons, thus the measured lifetimes correspond to those of a cascade instead of being the individual excited state lifetimes. To minimize the cascade effect in 2PPE measurements, low excited electron distribution and thus low laser fluences should be used (∼0.3 nJ/pulse in [20], for example).

Experimental $e - e$ relaxation times can be very useful to estimate the screening parameter value q_s. $e - e$ collision integral and thus theoretical $e - e$ relaxation time strongly depend on q_s. By comparing calculated $e - e$ relaxation times with measured ones, phenomenological values of q_s can be determined.

Table 3. 2PPE measurement experimental conditions of reference [20] for an Ag film.

Laser Fluence	0.3 nJ/pulse
Spot size	150 μm
Photon energy	3.3 eV
Penetration depth (at 3.3 eV)	150 Å
Excited volume	3×10^{-10} cm^3
Absorption coefficient	10%
Pulse fluence	1.5 μJ/cm^2

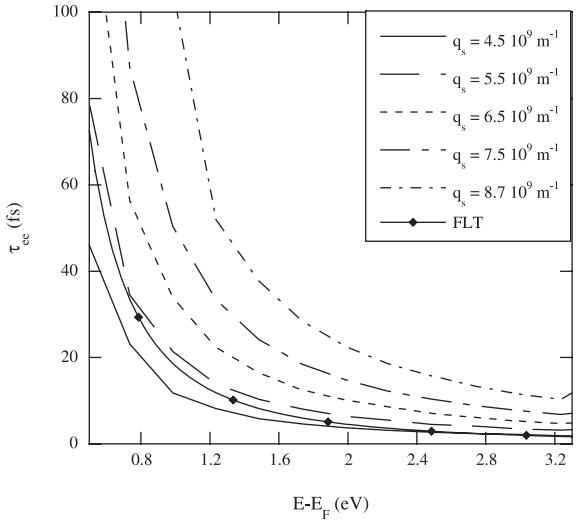

Fig. 17. Relaxation times $\tau_{ee}(E - E_F)$ vs. $E - E_F$ for Ag corresponding to different values of the screening parameter q_s. The prediction of the FLT is also reported.

Theoretical $e - e$ relaxation times have been obtained by fitting the eedf(E) slopes versus time with an exponential decay function $(\exp(-at) + b)$ in the temporal range in which the decay occurs. These calculations have been performed for different screening parameters q_s in the range near the value predicted by the Thomas-Fermi model ($q_s = q_{TF} = 8.7 \times 10^9$ m^{-1} for Ag). The laser perturbation conditions chosen correspond to those used in 2PPE measurement experimental conditions of reference [20] (see Tab. 3). According to these values, the imposed total energy absorbed by the films was

$$\begin{aligned} u_{abs} &= \frac{10}{100} \times \frac{1.5\,\mu\text{J/cm}^2}{150 \times 10^{-10}\ \text{m}} \\ &= 0.1 \times \frac{1.5 \times 10^{-2}\ \text{J/m}^2}{150 \times 10^{-10}\ \text{m}} = 10^5\ \frac{\text{J}}{\text{m}^3} \\ &= 0.1\ \frac{\text{J}}{\text{cm}^3} = 6.24 \times 10^{23}\ \frac{\text{eV}}{\text{m}^3}. \end{aligned} \tag{33}$$

These calculations have been performed by considering only $e - e$ collisions, by neglecting $e - p$ ones and fixing a constant Bose-Einstein phonon distribution at $T = 300$ K. A 20 fs laser pulse has been used. This choice has been arbitrary, since $e - e$ thermalization times do not depend on laser pulse duration.

Figure 17 shows the calculated relaxation times $\tau_{ee}(E - E_F)$ vs. $(E - E_F)$ for Ag for different values of q_s (in the range 4.5–8.7 $\times 10^9$ m^{-1}). In this figure, $e - e$ relaxation times predicted by the Fermi liquid theory are also reported. All the curves are characterized by the same dependence

$$\tau_{ee}^{-1} \propto K(E - E_F)^2 \tag{34}$$

in line with the result predicted by the Fermi liquid theory (Eq. (17)). The constant K and thus the absolute values of $\tau_{ee}(E - E_F)$ depend on the value used for the screening parameter. In particular, the larger the q_s values, the longer the relaxation.

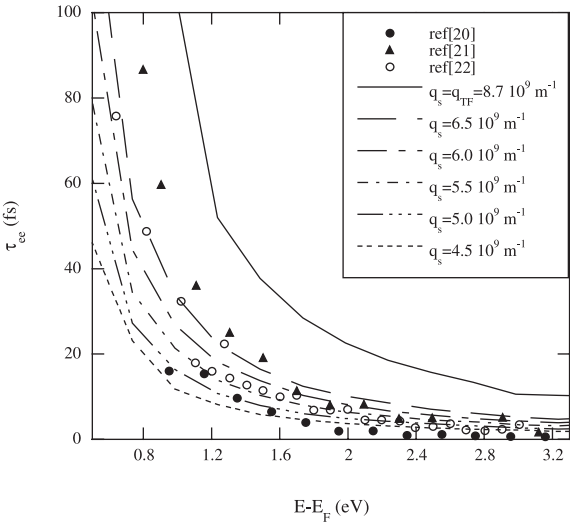

Fig. 18. Comparison between calculated relaxation times at different q_s values and experimental ones obtained in references [20–22].

Fig. 19. Free electron model. At $T = 0$ K, only the levels with $E < E_F$ are occupied.

These calculated $e-e$ relaxation times $\tau_{ee}(E-E_F)$ can be directly compared to the corresponding experimental values (see Fig. 18).

As we can see, the screening parameter value q_{TF} overestimates the $e - e$ relaxation times. This occurs since the dynamical phenomenon of $e-e$ screening is described with the static approximation by the Thomas-Fermi model. Thus, to have $e - e$ relaxation times comparable to experimental ones, smaller values of the screening parameter should be used, in particular, in the range 4.5×10^9 m^{-1}–6.5×10^9 m^{-1}. In the presented calculations, an intermediate screening parameter value of 5.5×10^9 m^{-1} has been used.

4.8 Photoemitted electron energy distribution

From the conduction band electron energy distribution, the photoemitted electron energy distribution can be calculated.

According to Figure 19, to escape from the metal, a free electron should have an energy on the direction

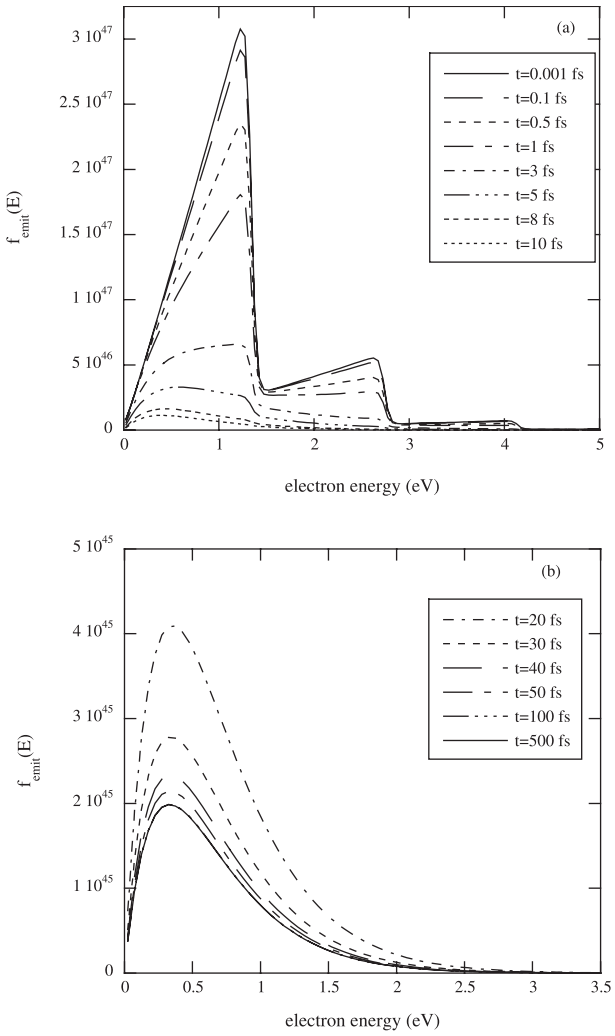

Fig. 20. Energy distribution function of the photoemitted electrons in the temporal range (a) [0.001–10] fs and (b) [20–500] fs.

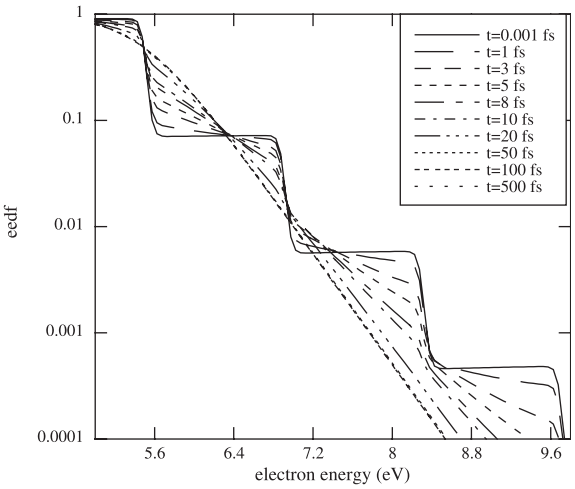

Fig. 21. Time evolution of the internal electron distribution from which the photoemitted electron distribution of Figure 20 has been calculated.

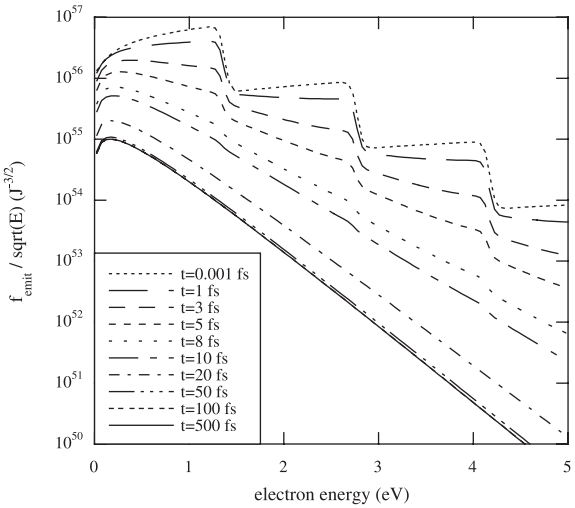

Fig. 22. Energy distribution function of the photoemitted electrons of Figure 20 divided by the square of the electron energy.

normal to the surface larger than $E_S = \Phi + E_F$, where Φ is the work function.

Thus, if z is the direction perpendicular to the surface, the electron should have a momentum $p_z \geqslant p_z^0$ where

$$\frac{(p_z^0)^2}{2m} = E_s. \tag{35}$$

The photoemitted electron total number can be written (see Appendix B)

$$N_{emit} = \frac{4\pi m}{h^3} \int_{E_S}^{\infty} (E - E_s) f(E) dE \tag{36}$$

while the photoemitted electron energy distribution is given by

$$f_{emit}(E) = \frac{4\pi m}{h^3} (E - E_s) f(E). \tag{37}$$

As an example, Figures 20a and 20b show the time evolution of the photoemitted electron distribution in the temporal range (a) [0.001–10] fs and (b) [20–500] fs, in the case in which the Ag film is submitted to an instantaneous laser perturbation with $u_{abs} = 4.17062 \times 10^8$ J/m^3 ($\Delta T_{exc} = 2700$ K). In the calculation, only $e - e$ collisions have been included. In Figure 21, the corresponding internal electron energy distribution function is shown.

The internal electron distribution step shape, due to the laser perturbation, creates some peaks in the photoemitted electron distribution. During the internal electron relaxation, such peaks are rounded off and when the internal distribution thermalizes to the Fermi-Dirac distribution, the photoemitted electron distribution reaches the Boltzmann one. Figure 22 shows the photoemitted electron distribution divided by the square of the electron energy. In this representation, the Boltzmann distribution is a straight line. Such equilibrium distribution is reached already at $t = 500$ fs, i.e. at the same instant at which

the internal electron distribution thermalized to a Fermi-Dirac distribution.

The total number of photoemitted electrons in this conditions is 3.0091×10^{15} m^{-3}, which correspond approximately to a fraction 10^{-14} of the conduction band electrons.

5 Conclusion

The electron and phonon relaxation dynamics in a metal film subjected to a femtosecond laser pulse have been theoretically investigated. For this reason, a numerical solution of a system of two Boltzmann equations, one for the electrons and the other for the phonons, has been performed. In the electron Boltzmann equation, the collision integrals due to electron-electron and electron-phonon collisions and a laser perturbation term have been considered. In the phonon Boltzmann equation, instead, only the electron-phonon collision integral has been included. The theoretical model has been applied to noble metals, in particular Ag, since their electronic band structure can be well described by the free electron model.

The results have shown the non-equilibrium behaviour of both electron and phonon distributions and the main features of electron and phonon relaxation dynamic after the femtosecond laser perturbation. Since electron-electron collisions do not thermalize the electron gas on a time scale shorter than the laser pulse duration, the electron distribution is in a strong non-equilibrium condition and the TTM approach, which describes the electrons through an equilibrium temperature, cannot be applied. Only the microscopic kinetic approach based on the solution of the Boltzmann equation can provide an accurate description of this phenomenology. Experimental comparison with 2PPE measurements is possible. These experiments provide direct measurements of the electron distribution relaxation. The comparison shows a qualitative agreement, confirming of the theoretical model viability. 2PPE experiments give also a measurement of $e-e$ relaxation times, which, compared to theoretical ones, can provide a screening parameter value q_s estimation to be used in theoretical model.

Although the TTM approach is generally inadequate for electron and phonon relaxation dynamics description when a femtosecond laser pulse is used, the electron cooling can be well described by the TTM if sufficiently laser energy is injected into the metal, see also the work of Rethfeld et al. [10].

Moreover, our theoretical model has shown that, in general, non-equilibrium electron distributions slow down $e-p$ energy exchange. This result has been confirmed also experimentally in references [5,6] through pump-and-probe reflectivity and transmissivity measurements.

Finally, from the non-equilibrium internal electron distributions, the energy distribution of the photoemitted electrons has been calculated. The transient non-equilibrium behaviour of the internal electron distribution creates some peaks in the photoemitted electron distribution. During the internal electron thermalization, such peaks are rounded off and the photoemitted electron distribution is finally driven towards a Boltzmann distribution, corresponding to a thermalized internal electron distribution.

Future works should be devoted to the improvement of the presented theoretical model. First of all, a more accurate laser absorption model can be developed, taking into account photon absorption mediated by electron-ion collisions [9,10]. Moreover, transport effect should be included into the model together with a spatial coordinate. Laser intensity can be increased up to the laser damage threshold in order to investigate also the ablation conditions. Finally, the effect of non-equilibrium electron distributions over optical properties such as refraction index and dielectric constant can be calculated in order to have direct comparison also with the experimental results of pump-and-probe measurements.

This work has been partially supported by MIUR PRIN 2005 N. 2005039049_005.

Appendix A: Conservation properties

A.1 Electron density conservation condition

To conserve electron density, the following condition should be verified (see Eq. (22))

$$\frac{dn_e}{dt} = \int D_e(E_e)\frac{df(E_e)}{dt}dE_e = \int D_e(E_e)\left[\left.\frac{df(E_e)}{dt}\right|_{ee} + \left.\frac{df(E_e)}{dt}\right|_{ep}\right]dE_e = 0 \tag{A.1}$$

thus

$$\begin{cases} \int D_e(E_e)\left.\dfrac{df(E_e)}{dt}\right|_{ee} dE_e = 0 \\ \int D_e(E_e)\left.\dfrac{df(E_e)}{dt}\right|_{ep} dE_e = 0 \end{cases}. \tag{A.2}$$

By discretizing the electron energy, equation (A.2) becomes

$$\begin{cases} \sum\limits_k D_e^k \left.\dfrac{df_k}{dt}\right|_{ee} dE_k = 0 \\ \sum\limits_k D_e^k \left.\dfrac{df_k}{dt}\right|_{ep} dE_k = 0 \end{cases}. \tag{A.3}$$

By using the matrix representation form for both the $e-e$ and $e-p$ collision integrals one obtains:

$$\left.\frac{df_k}{dt}\right|_{ee} = \sum_j M_{kj}^{ee} f_j, \quad \left.\frac{df_k}{dt}\right|_{ep} = \sum_j M_{kj}^{ep} f_j. \tag{A.4}$$

Substituting equation (A.4) in (A.3) and supposing the electron energy grid uniform ($dE_k = dE$), the electron density condition becomes:

$$\sum_k D_e^k M_{kj}^{ee} = 0, \quad \sum_k D_e^k M_{kj}^{ep} = 0. \tag{A.5}$$

Thus according to equation (A.5), both $e-e$ and $e-p$ matrix must be constructed in such a way that, once fixed a column j, the sum over the corresponding row elements k, each one multiplied by the density of state D_e^k, must be zero.

Let focus on $e-e$ collisions and consider a scattering event in which the involved electrons have the following energies, E_1, E_2, E_3 and E_4 corresponding to the following indexes k_1, k_2, k_3 and k_4 in the electron energy axis.

According to equation (15), the $e-e$ scattering probability is proportional to the following constant:

$$C_{ee} = \frac{m^{5/2}}{2^{7/2}\pi^3\hbar^6}\frac{Se^4}{\varepsilon^2} \times \left[\frac{q}{2q_s^2(q^2+q_s^2)} + \frac{1}{2q_s^2}\arctan g\left(\frac{q}{q_s}\right)\right]\Bigg|_{q_{\min}}^{q_{\max}}. \quad (A.6)$$

Let introduce the following terms:

$$\begin{aligned} a_1 &= C_{ee} f(E_2)\left[1-f(E_3)\right]\left[1-f(E_4)\right] \\ a_2 &= C_{ee} f(E_1)\left[1-f(E_3)\right]\left[1-f(E_4)\right] \\ a_3 &= C_{ee} f(E_4)\left[1-f(E_1)\right]\left[1-f(E_2)\right] \\ a_4 &= C_{ee} f(E_3)\left[1-f(E_1)\right]\left[1-f(E_2)\right]. \end{aligned} \quad (A.7)$$

In the process for which $E_1, E_2 \to E_3, E_4$, the matrix elements $M^{ee}_{k_1k_1}$ and $M^{ee}_{k_2k_2}$ are given by:

$$M^{ee}_{k_1k_1} = -\frac{1}{\sqrt{E_1}}a_1, \quad M^{ee}_{k_2k_2} = -\frac{1}{\sqrt{E_2}}a_2. \quad (A.8)$$

The elements $M^{ee}_{k_3k_1}$, $M^{ee}_{k_4k_1}$ and $M^{ee}_{k_3k_2}$, $M^{ee}_{k_4k_2}$ can be calculated by imposing the condition (Eq. (A.5)), thus:

$$\begin{aligned} D_e^{k_1}M^{ee}_{k_1k_1} + D_e^{k_2}M^{ee}_{k_3k_1} + D_e^{k_4}M^{ee}_{k_4k_1} &= 0 \\ D_e^{k_2}M^{ee}_{k_2k_2} + D_e^{k_3}M^{ee}_{k_3k_2} + D_e^{k_4}M^{ee}_{k_4k_2} &= 0. \end{aligned} \quad (A.9)$$

Consequently

$$\begin{aligned} M^{ee}_{k_1k_1} &= -\frac{D_e^{k_3}}{D_e^{k_1}}M^{ee}_{k_3k_1} - \frac{D_e^{k_4}}{D_e^{k_1}}M^{ee}_{k_4k_1} \\ M^{ee}_{k_2k_2} &= -\frac{D_e^{k_3}}{D_e^{k_2}}M^{ee}_{k_3k_2} - \frac{D_e^{k_4}}{D_e^{k_2}}M^{ee}_{k_4k_2}. \end{aligned} \quad (A.10)$$

Since $D_e^k \propto \sqrt{E_k}$

$$\begin{aligned} M^{ee}_{k_1k_1} &= -\frac{\sqrt{E_3}}{\sqrt{E_1}}M^{ee}_{k_3k_1} - \frac{\sqrt{E_4}}{\sqrt{E_1}}M^{ee}_{k_4k_1} \\ M^{ee}_{k_2k_2} &= -\frac{\sqrt{E_3}}{\sqrt{E_2}}M^{ee}_{k_3k_2} - \frac{\sqrt{E_4}}{\sqrt{E_2}}M^{ee}_{k_4k_2}. \end{aligned} \quad (A.11)$$

Since the matrix elements $M^{ee}_{k_1k_1}$ and $M^{ee}_{k_2k_2}$ are given by equation (A.8), the condition (A.11) is true only if we impose that

$$\begin{aligned} M^{ee}_{k_3k_1} &= \frac{1}{2}\frac{1}{\sqrt{E_3}}a_1, \quad M^{ee}_{k_4k_1} = \frac{1}{2}\frac{1}{\sqrt{E_4}}a_1 \\ M^{ee}_{k_3k_2} &= \frac{1}{2}\frac{1}{\sqrt{E_3}}a_2, \quad M^{ee}_{k_4k_2} = \frac{1}{2}\frac{1}{\sqrt{E_4}}a_2. \end{aligned} \quad (A.12)$$

If we consider all the scattering events that involve the states E_1, E_2, E_3 and E_4, also the process in which $E_3, E_4 \to E_1, E_2$ should be taken into account. This process must be treated in the same way as previous. Thus we can write:

$$\begin{aligned} M^{ee}_{k_3k_3} &= -\frac{1}{\sqrt{E_3}}a_3, \quad M^{ee}_{k_4k_4} = -\frac{1}{\sqrt{E_4}}a_4 \\ M^{ee}_{k_1k_3} &= -\frac{1}{2\sqrt{E_1}}a_3, \quad M^{ee}_{k_2k_3} = -\frac{1}{2\sqrt{E_2}}a_3 \\ M^{ee}_{k_1k_4} &= -\frac{1}{2\sqrt{E_1}}a_4, \quad M^{ee}_{k_2k_4} = -\frac{1}{2\sqrt{E_2}}a_4. \end{aligned} \quad (A.13)$$

Finally, using the matrix representation, the direct and inverse scattering processes $E_1, E_2 \leftrightarrow E_3, E_4$ are characterized by the following matrix elements:

$$\begin{pmatrix} -\frac{1}{\sqrt{E_1}}a_1 & 0 & \frac{1}{2\sqrt{E_1}}a_3 & \frac{1}{2\sqrt{E_1}}a_4 \\ 0 & -\frac{1}{\sqrt{E_2}}a_2 & \frac{1}{2\sqrt{E_2}}a_3 & \frac{1}{2\sqrt{E_2}}a_4 \\ \frac{1}{2\sqrt{E_3}}a_1 & \frac{1}{2\sqrt{E_3}}a_2 & -\frac{1}{\sqrt{E_3}}a_3 & 0 \\ \frac{1}{2\sqrt{E_4}}a_1 & \frac{1}{2\sqrt{E_4}}a_2 & 0 & -\frac{1}{\sqrt{E_4}}a_4 \end{pmatrix}. \quad (A.14)$$

Concerning the $e-p$ interaction, according to equation (A.5), the $e-p$ matrix must be constructed imposing:

$$M^{ep}_{jj} = -\sum_k \frac{D_e^k}{D_e^j}M^{ep}_{kj}, \; M^{ep}_{kk} = -\sum_j \frac{D_e^j}{D_e^k}M^{ep}_{jk}. \quad (A.15)$$

A.2 Detailed balance principle

Concerning $e-e$ collisions, the explicit expression of the collision integral, in equation (9), has been constructed in such a way that the detailed balance principle is already verified.

In the case of $e-p$ collisions, instead, some restrictions should be imposed. If $P(\mathbf{k}\to\mathbf{j},\mathbf{q})$ and $P(\mathbf{j},\mathbf{q}\to\mathbf{k})$ represent, respectively, the probability of the direct and inverse process of phonon emission and absorption, which involve phonons with wave vector $\mathbf{q}$ and electrons with wave vector $\mathbf{k}$ and $\mathbf{j}=\mathbf{k}-\mathbf{q}$, the detailed balance principle imposes that at equilibrium

$$P(\mathbf{k}\to\mathbf{j},\mathbf{q}) = P(\mathbf{j},\mathbf{q}\to\mathbf{k}). \quad (A.16)$$

Since $P(\mathbf{k}\to\mathbf{j},\mathbf{q})$ and $P(\mathbf{j},\mathbf{q}\to\mathbf{k})$ can be written in the following way:

$$P(\mathbf{k}\to\mathbf{j},\mathbf{q}) = \Omega_{kk} f_k\left(1-f_j\right)\left(1+N_q\right)D_q dE_q \quad (A.17)$$

$$P(\mathbf{j},\mathbf{q}\to\mathbf{k}) = \Omega_{kj} f_j\left(1-f_k\right)N_q D_q dE_q. \quad (A.18)$$

Imposing equation (A.16) and the Fermi-Dirac and Bose-Einstein distribution at the same temperature T for the electron and phonon gas, the following relation between Ω_{kk} and Ω_{kj} can be deduced:

$$\Omega_{kk} = e^{\frac{(E_k-E_j-E_q)}{KT}}\Omega_{kj}. \quad (A.19)$$

This equation, however, is based on the assumption of a macroscopic equilibrium temperature T and cannot be used in non-equilibrium conditions. Thus, an alternative way to impose the detailed balance principle should be found.

One way could be the definition of a local electron equilibrium temperature (or punctual temperature) for each electron energy interval k and the imposition of a local detailed balancing principle. By fixing a particular kth interval, the corresponding punctual temperature T_k^{punct} can be calculated from the kth interval electron distribution function value f_k, imposing a Fermi-Dirac distribution, i.e.

$$f_k = \frac{1}{e^{\frac{E_k - E_F}{KT_k^{punct}}} + 1} \Rightarrow T_k^{punct} = \frac{1}{K} \frac{E_k - E_F}{\ln\left(\frac{1-f_k}{f_k}\right)}. \quad \text{(A.20)}$$

This calculation could be done only for the electron energy intervals for which $f_k \neq 1$. Once defined the kth punctual equilibrium temperature T_k^{punct}, let fix our attention over one single direct process of phonon emission, in which electrons in the kth interval emit one phonon with energy E_q in the qth phonon energy axis interval. Phonon energies are of the order of meV, thus their maximum value ($E_q^{\max}$) is, generally, less than the electron energy interval width dE_e $\left(\frac{E_q^{\max}}{dE_e} < 1\right)$. As a consequence, kth electrons will move toward $j\text{th} = (k-1)\text{th}$ interval. If E_k represents the electron energy corresponding to the kth interval centre, after a phonon emission process, only electrons in the energy range $[E_1, E_2] = \left[E_k - \frac{dE_e}{2}, E_k - \frac{dE_e}{2} + E_q\right]$ will change interval, giving a nonzero transition probability contribution. These electrons will move into $j\text{th} = (k-1)\text{th}$ energy range, in particular, in the interval $[E_3, E_1] = \left[E_j + \frac{dE_e}{2} - E_q, E_j + \frac{dE_e}{2} = E_k - \frac{dE_e}{2}\right]$.

Symmetrically, for the absorption inverse process, there will be a nonzero contribution only for electrons of the $j\text{th} = (k-1)\text{th}$ interval with energies in the range $[E_3, E_1]$, which will move to kth interval energy range of $[E_1, E_2]$.

The total emission and absorption probability, which involve the kth and the jth intervals are proportional to the following integrals:

(a) emission

$$P(\mathbf{k} \to \mathbf{j}, \mathbf{q}) = \Omega_{kk} \frac{1}{dE} \int_{E_1}^{E_2} f_s \left(1 - f_z\right) \left(1 + N_q\right) D_q dE \quad \text{(A.21)}$$

(b) absorption

$$P(\mathbf{j}, \mathbf{q} \to \mathbf{k}) = \Omega_{kj} \frac{1}{dE} \int_{E_3}^{E_1} f_z \left(1 - f_s\right) N_q D_q dE \quad \text{(A.22)}$$

where f_s and f_z represent the electron distribution corresponding to the energy $E_s \in [E_1, E_2]$ and $E_z \in [E_3, E_1]$. Using the average theorem, the integrals in equations (A.21) and (A.22) can be approximated by:

$$P(\mathbf{k} \to \mathbf{j}, \mathbf{q}) \approx \Omega_{kk} f_{\bar{s}} \left(1 - f_{\bar{z}}\right) \left(1 + N_q\right) D_q \frac{E_q}{dE} \quad \text{(A.23)}$$

$$P(\mathbf{j}, \mathbf{q} \to \mathbf{k}) \approx \Omega_{kj} f_{\bar{z}} \left(1 - f_{\bar{s}}\right) N_q D_q \frac{E_q}{dE} \quad \text{(A.24)}$$

where $f_{\bar{s}}, f_{\bar{z}}$ represent the electron distributions corresponding to the average energy values $E_{\bar{s}}, E_{\bar{z}}$ of the $[E_1, E_2]$ and $[E_3, E_1]$ intervals, respectively. For an estimation of the $f_{\bar{s}}, f_{\bar{z}}$ values, we can use Fermi-Dirac distributions with the punctual electron temperature of the intervals in which $E_{\bar{s}}$, $E_{\bar{z}}$ fall. Thus, if T_k and T_j are the punctual electron temperatures of the kth and the jth intervals, respectively, $f_{\bar{s}}, f_{\bar{z}}$ are:

$$f_{\bar{s}} = \frac{1}{e^{\frac{E_{\bar{s}} - E_F}{KT_k}} + 1}, \quad f_{\bar{z}} = \frac{1}{e^{\frac{E_{\bar{z}} - E_F}{KT_j}} + 1}. \quad \text{(A.25)}$$

According equation (A.16)

$$\Omega_{kk} f_{\bar{s}} \left(1 - f_{\bar{z}}\right) \left(1 + N_q\right) = \Omega_{kj} f_{\bar{z}} \left(1 - f_{\bar{s}}\right) N_q$$
$$\Rightarrow \Omega_{kk} = \frac{f_{\bar{z}} \left(1 - f_{\bar{s}}\right) N_q}{f_{\bar{s}} \left(1 - f_{\bar{z}}\right) \left(1 + N_q\right)} \Omega_{kj}. \quad \text{(A.26)}$$

If we substitute the $f_{\bar{s}}$, $f_{\bar{z}}$ expressions given by equation (A.25) into equation (A.26) and if we suppose that the phonon distribution N_q is characterized by a Bose-Einstein distribution at a temperature T_p, we have that equation (A.26) now becomes:

$$\Omega_{kk} = e^{\frac{E_{\bar{z}} - E_F}{kT_j}} e^{\frac{E_{\bar{s}} - E_F}{kT_k}} e^{-\frac{E_p}{kT_p}} \Omega_{kj}. \quad \text{(A.27)}$$

Using equations (A.23), (A.24) and (A.27), in the calculation of each emission and absorption probability, the detailed balance principle will be locally and, consequently, also globally valid.

A.3 Total energy conservation condition

Concerning $e-e$ collision integral, it can be simply proved that the $e-e$ matrix constructed according (A.14) conserves total electron energy as well. In particular, that for each j the following condition holds:

$$\sum_k E_k D_k M_{kj}^{ee} = 0. \quad \text{(A.28)}$$

Concerning $e-p$ collision integral, instead, the total energy conservation condition must be imposed. To this purpose, $e-p$ phonon distribution changes have been calculated from the $e-p$ electron distribution changes using total energy conservation condition. If ΔE_e represents the electron energy change due to $e-p$ processes which involve phonons with q momentum, and ΔE_q the corresponding phonon energy change, according to the total energy conservation condition

$$\Delta E_q = -\Delta E_e. \quad \text{(A.29)}$$

Since

$$\Delta E_e = \sum_k E_k D_k^e \left.\frac{df_k}{dt}\right|_{ep} dE_k \tag{A.30}$$

and

$$\Delta E_q = E_q D_q \left.\frac{dN_q}{dt}\right|_{ep} dE_q. \tag{A.31}$$

The phonon distribution change must be calculated from the electron distribution changes through

$$\left.\frac{dN_q}{dt}\right|_{ep} = -\frac{\Delta E_e}{E_q D_q dE_q}. \tag{A.32}$$

In particular, by considering the phonon emission and absorption processes, which involve only electrons from kth and jth ($j = k-1$, $j < k$) intervals and phonons with energy E_q, after different mathematical passages, one obtain

$$\left.\frac{dN_q}{dt}\right|_{ep} = \Omega^+(N_q+1) - \Omega^- N_q \tag{A.33}$$

with

$$\begin{aligned}\Omega^+ &= C_{ep} dE_e f_{\bar{s}}\,(1-f_{\bar{z}})\\ \Omega^- &= C_{ep} dE_e f_{\bar{z}}\,(1-f_{\bar{s}})\end{aligned} \tag{A.34}$$

where, Ω^+ and Ω^- represents the phonon emission and absorption total rate, respectively, and

$$C_{ep} = D_e^k \Omega_{kk} = D_e^k \Omega_{kj}. \tag{A.35}$$

Appendix B: Photoemitted electrons

If v_z and p_z are, respectively, the electron velocity and momentum in the z-direction, perpendicular to metal surface and $n(p_z)dp_z$ the number of electrons per unit volume with momentum between p_z and $p_z + dp_z$, the electrons which arrives to the surface per unit time and unit surface is given by $v_z n(p_z) dp_z$.

In the hypothesis of an isotropic electron distribution, the number of possible states, per unit volume, in the element $dp_x dp_y dp_z$ of the momentum space is given by:

$$\frac{2dp_x dp_y dp_z}{h^3}. \tag{B.1}$$

Thus the number of electrons with momentum between p_x, $p_x + dp_x$; p_y, $p_y + dp_y$; p_z, $p_z + dp_z$ is

$$n(p_x,p_y,p_z)dp_x dp_y dp_z = \frac{2}{h^3} f(E) dp_x dp_y dp_z \tag{B.2}$$

where $f(E)$ represents the electron energy distribution function with $E = \frac{p_x^2+p_y^2+p_z^2}{2m}$.

Thus, the total number of electrons emitted by the surface is:

$$\begin{aligned}N_{emit} &= \int_{p_z^0}^{\infty}\int_{-\infty}^{+\infty}\int_{-\infty}^{+\infty} \frac{p_z}{m} n(p_x,p_y,p_z) dp_x dp_y dp_z\\ &= \frac{2}{mh^3}\int_{p_z^0}^{\infty}\int_{-\infty}^{+\infty}\int_{-\infty}^{+\infty} p_z f(E) dp_x dp_y dp_z.\end{aligned} \tag{B.3}$$

Let us consider the following quantities $p_\perp = p_z$, $p_\parallel = \sqrt{p_x^2+p_y^2}$, $E_\perp = \frac{p_\perp^2}{2m}$, $E_\parallel = \frac{p_\parallel^2}{2m}$ and $E = E_\perp + E_\parallel$. The double integral over the x and y momentum components can be calculated in the following way:

$$\int_{-\infty}^{+\infty}\int_{-\infty}^{+\infty} dp_x dp_y = \int_0^{\infty} p_\parallel dp_\parallel \int_0^{2\pi} d\varphi = 2\pi \int_0^{\infty} p_\parallel dp_\parallel. \tag{B.4}$$

Thus equation (B.3) becomes

$$N_{emit} = \frac{4\pi}{mh^3}\int_{p_z^0}^{\infty}\int_0^{\infty} p_\perp p_\parallel f(E) dp_\perp dp_\parallel. \tag{B.5}$$

Since, $p_\perp = p\cos\vartheta$ and $p_\parallel = p\sin\vartheta$

$$N_{emit} = \frac{4\pi}{mh^3}\int_{p_z^0}^{\infty} f(E) p^3 dp \int_0^{\vartheta_{\max}} \cos\vartheta \sin\vartheta d\vartheta \tag{B.6}$$

where $\vartheta_{\max} = ar\cos\frac{p_z^0}{p}$. Thus,

$$\int_0^{\vartheta_{\max}} \cos\vartheta\sin\vartheta d\vartheta = \frac{1}{2}\left(\frac{p^2-(p_z^0)^2}{p^2}\right) \tag{B.7}$$

substituting equation (B.7) into equation (B.6)

$$\begin{aligned}N_{emit} &= \frac{4\pi}{mh^3}\frac{1}{2}\int_{p_z^0}^{\infty} p^3 \frac{p^2-(p_z^0)^2}{p^2} f(E) dp\\ &= \frac{2\pi}{mh^3}\int_{p_z^0}^{\infty} p\left(p^2-(p_z^0)^2\right) f(E) dp.\end{aligned} \tag{B.8}$$

In terms of electron energy, equation (B.8) becomes

$$N_{emit} = \frac{4\pi m}{h^3}\int_{E_S}^{\infty} (E-E_s) f(E) dE. \tag{B.9}$$

References

1. A. Bogaerts, Z. Chen, R. Gijbels, A. Vertes, Spectrochim. Acta B **58**, 1867 (2003)
2. S.I. Anisimov, A.M. Bonch-Bruevich, M.A. El'yashevich, Ya. A. Imas, N.A. Pavlenko, G.R. Romanov, Zh. Tekh. Fiz. **36**, 1273 (1966) [Sov. Phys. Tech. Phys. **11**, 945 (1967)]
3. S.I. Anisimov, B.L. Kapeliovitch, T.L. Perel'man, Zh. Eksp. Teor. Fiz. **66**, 776 (1974) [Sov. Phys. JETP **39**, 375 (1974)]
4. C.K. Sun, F. Vallée, L.H. Acioli, E.P. Ippen, J.G. Fujimoto, Phys. Rev. B **48**, 12365 (1993)
5. N. Del Fatti, C. Voisin, M. Achermann, S. Tzortzakis, D. Christofilos, F. Vallée, Phys. Rev. B **61**, 16956 (2000)
6. R.H.M. Groeneveld, R. Sprik, Phys. Rev. B **45**, 5079 (1992)
7. D. Bejan, R. Raseev, Phys. Rev. B **55**, 4250 (1997)
8. V.E. Gusev, O.B. Wright, Phy. Rev. B **57**, 2878 (1998)
9. A.V. Lugovskoy, I. Bray, Phys. Rev. B **60**, 3279 (1999)
10. B. Rethfeld, A. Kaiser, M. Vicanek, G. Simon, Phys. Rev. B **65**, 214303 (2002)
11. S. Longo, L.D. Pietanza, F.A. Tassielli, M. Capitelli, Laser, Particle Beams **20**, 285 (2002)

12. L.D. Pietanza, G. Colonna, S. Longo, M. Capitelli, Thin Solid Film **453**, 512 (2004)
13. L.D. Pietanza, G. Colonna, S. Longo, M. Capitelli, Appl. Phys. A **79**, 1047 (2004)
14. L.D. Pietanza, G. Colonna, M. Capitelli, Appl. Surf. Sci. **248**, 103 (2005)
15. W.S. Fann, R. Storz, H.K. Tom, J. Bokor, Phys. Rev. Lett. **68**, 2834 (1992)
16. W.S. Fann, R. Storz, H.K. Tom, J. Bokor, Phys. Rev. B **46**, 13592 (1992)
17. M. Lisowski, P.A. Loukakos, U. Bovensiepen, J. Stahler, C. Gahl, M. Wolf, Appl. Phys. A **78**, 165 (2004)
18. M. Lisowski, P.A. Loukakos, U. Bovensiepen, M. Wolf, Appl. Phys. A **79**, 739 (2004)
19. M. Lisowski, P.A. Loukakos, M. Melnikov, I. Radu, L. Ungureanu, M. Wolf, U. Bovensiepen, Phys. Rev. Lett. **95**, 137402 (2005)
20. M. Aeschlimann, M. Bauer, S. Pawlik, Chem. Phys. **205**, 127 (1996)
21. M. Aeschlimann, M. Bauer, S. Pawlik, W. Weber, R. Burgermeister, D. Oberli, H.C. Siegmann, Phys. Rev. Lett. **79**, 5158 (1997)
22. M. Wolf, M. Aeschlimann, Phys. B1 **54**, 145 (1998)
23. M. Bauer, M. Aeschlimann, J. Electron Spectr. Rel. Phenom. **124**, 225 (2002)
24. S.Ogawa, H. Nagano, H. Petek, Phys. Rev. B **55**, 10869 (1997)
25. E. Knoesel, A. Hotzel, M. Wolf, Phys. Rev. B **57**, 12812 (1998)
26. J. Cao, Y. Gao, H.E. Elayed-Ali, R.J.D. Miller, D.A. Mantell, Phys. Rev. B **58**, 10948 (1998)
27. M. Bonn, D.N. Denzel, S. Funk, M. Wolf, S.-S. Wellershoff, J. Hohlfeld, Phys. Rev. B **61**, 1101 (2000)
28. C.K. Sun, F. Vallée, L.H. Acioli, E.P. Ippen, J.G. Fujimoto, Phys. Rev. B **50**, 15337 (1994)
29. R.H.M. Groeneveld, R. Sprik, A. Lagendijk, Phys. Rev. B **51**, 11433 (1995)
30. R.W. Schoenlein, W.Z. Lin, J.G. Fujimoto, G.L. Eesley, Phys. Rev. Lett. **58**, 1680 (1987)
31. H.E. Elsayed-Ali, T.B. Norris, M.A. Pessot, G.A. Mourou, Phys. Rev. Lett. **58**, 1212 (1987)
32. H.E. Elsayed-Ali, T. Juhasz, G.O. Smith, W.E. Bron, Phys. Rev. B **43**, 4488 (1990)
33. S.D. Brorson, A.Kazeroonian, J.S. Modera, D.W. Face, T.K. Cheng, E.P. Ippen, M.S. Dresselhaus, G. Dresselhaus, Phys. Rev. Lett. **64**, 2172 (1990)
34. S.D. Brorson, J.G. Fujimoto, E.P. Ippen, Phys. Rev. Lett. **59**, 1962 (1987)
35. C. Suarez, W.E. Bron, T. Juhasz, Phys. Rev. Lett. **75**, 4536 (1995)
36. N. Del Fatti, R. Bouffanais, F. Vallée, C. Flytzanis, Phy. Rev. Lett. **81**, 922 (1998)
37. R. Rosei, D.W. Lynch, Phys. Rev. B **5**, 3883 (1972)
38. R. Rosei, Phys. Rev. B **10**, 474 (1974)
39. R. Rosei, C.H. Culp, J.H. Weaver, Phys. Rev. B **10**, 484 (1974)
40. R. Rosei, F. Antonangeli, U.M. Grassano, Surf. Sci. **37**, 689 (1973)
41. N.W. Ashcroft, N.D. Mermin, *Solid State Physics* (Holt Saunders International Editions, 1976)
42. D. Pines, *Elementary excitations in solids* (W.A. Benjamin Inc., New York, 1963)
43. D. Pines, P. Nozières, W.A. Benjamin Inc., New York (1966)
44. S.L. Adler, Phys. Rev. **130**, 1654 (1963)
45. W.E. Lawrence, Phys. Rev. B **13**, 5316 (1976)
46. D.R. Penn, Phys. Rev. B **22**, 2677 (1980)
47. J.H. Collet, Phys. Rev. B **47**, 10279 (1993)
48. D.W. Snoke, W.W. Ruhle, Y.C. Lu, E. Bauser, Phys. B **45**, 10979 (1992)
49. D.W. Snoke, J.P. Wolfe, Phys. Rev. B **39**, 4030 (1989)
50. J.M.Ziman, *Electrons and phonons* (Clarendon Press, Oxford, 1960)
51. P.B. Allen, Phys. Rev. Lett. **59**, 1460 (1987)
52. G. Colonna, Suppl. Rend. Circ. Mat. Palermo II **57**, 159 (1998)